

Efficient Sparse Coding using Hierarchical Riemannian Pursuit

Ye Xue, Vincent Lau, and Songfu Cai

Abstract

Sparse coding is a class of unsupervised methods for learning a sparse representation of the input data in the form of a linear combination of a dictionary and a sparse code. This learning framework has led to state-of-the-art results in various image and video processing tasks. However, classical methods learn the dictionary and the sparse code based on alternative optimizations, usually without theoretical guarantees for either optimality or convergence due to non-convexity of the problem. Recent works on sparse coding with a complete dictionary provide strong theoretical guarantees thanks to the development of the non-convex optimization. However, initial non-convex approaches [1–4] learn the dictionary in the sparse coding problem sequentially in an atom-by-atom manner, which leads to a long execution time. More recent works [5–7] seek to directly learn the entire dictionary at once, which substantially reduces the execution time. However, the associated recovery performance is degraded with a finite number of data samples. In this paper, we propose an efficient sparse coding scheme with a two-stage optimization. The proposed scheme leverages the global and local Riemannian geometry of the two-stage optimization problem and facilitates fast implementation for superb dictionary recovery performance by a finite number of samples without atom-by-atom calculation. We further prove that, with high probability, the proposed scheme can exactly recover any atom in the target dictionary with a finite number of samples if it is adopted to recover one atom of the dictionary. An application on wireless sensor data compression is also proposed. Experiments on both synthetic and real-world data verify the efficiency and effectiveness of the proposed scheme. The codes to reproduce the experimental results are available online at <https://github.com/yokoxue/HRP>.

1 Introduction

In the era of big data, finding efficient data representation is crucial for both application and analysis, and sparse representation is one of the most popular data representations. With this representation, the high-dimensional data $\mathbf{y} \in \mathbb{R}^N$ can be expressed by $\mathbf{y} \approx \mathbf{D}^* \mathbf{x}^*$, where $\mathbf{x}^* \in \mathbb{R}^M$ is a sparse code (i.e., the number of non-zero entries of \mathbf{x}^* is much smaller than M) and the dictionary $\mathbf{D}^* \in \mathbb{R}^{N \times M}$ is a collection of M atoms $\{\mathbf{D}_{:,n}^* \in \mathbb{R}^{N \times 1}, n = 1, \dots, M\}$ that contains the compact information of \mathbf{y} . Sparse data representation has been increasingly used with success in many data processing and machine learning applications [8–11]. The performance of sparse-representation-based approaches hinges on using a proper dictionary, and many studies have been conducted to design efficient pre-specified dictionaries such as Fourier-based [12] and wavelet-based [13] dictionaries. However, such a generic approach may be unable to exploit domain-specific structures because the generic dictionary may not be the correct basis for a specific data set. Hence, the idea of learning the dictionary and the corresponding sparse code from a particular data set has emerged as a powerful framework, named *sparse coding*.

One typical formulation of sparse coding is [14]

$$\begin{aligned} & \underset{\mathbf{D}, \{\mathbf{x}_i\}_{i=1}^L}{\text{minimize}} && \sum_{i=1}^L \|\mathbf{y}_i - \mathbf{D} \mathbf{x}_i\|^2 \\ & \text{subject to} && \|\mathbf{x}_i\|_0 \leq T_0, \forall i, \end{aligned} \tag{1}$$

where $\|\cdot\|_0$ is the sparsity measure defined as the number of non-zero entries in the input and T_0 represents the predetermined maximum number of non-zero entries allowed in the sparse code. However, solving problem (1) is highly challenging due to the bilinear form of the received signal $\{\mathbf{y}_i\}_{i=1}^L$ with respect to the unknowns \mathbf{D} and $\{\mathbf{x}_i\}_{i=1}^L$ [15], as well as the discontinuous ℓ_0 norm constraint. Approaches that adopt alternative optimizations, such as the method of optimal directions (MOD) [16] and K-SVD [14], have achieved impressive practical success. Though these alternating iteration schemes generally can guarantee that the objective function value is decreasing, the generated sequence of iterates may diverge. As has been explicitly pointed out in [17], the sequence generated by K-SVD is not always convergent.

Moreover, the sparse coding step in such methods is computationally expensive [18]. Therefore, many variants of these methods have been proposed for efficient implementation [19, 20]. To alleviate the challenge brought by the ℓ_0 norm in problem (1), many other constraints, e.g., ℓ_1 norm, have been proposed to induce the sparsity [21–24]. In these works, the sparsity constraints are usually moved to the objective functions as the penalty term and the resulted problems are solved by alternative algorithms. In [18, 25], another alternative optimization scheme, named *sparsifying transform learning*, is proposed to learn the dictionary in the transform domain. Specifically, sparsifying transform learning deals with a cost function in which the modeling error is called the sparsification error and it improves the computation efficiency compared to the naive K-SVD [26]. In [18], the convergence of objectives is demonstrated for the sparsifying transform learning. However, the convergence of the variables is not provided.

Owing to the recent development of the non-convex optimization, several works have proposed solutions with rigorous justifications for optimality and convergence of sparse coding with a complete dictionary [1–7, 27]. The primary treatment is that, after simple preconditioning [1, 2], the sparse coding problem with a complete dictionary can be formulated as a problem with the dictionary restricted over the orthogonal group $\mathbb{O}(N) = \{\mathbf{Q} \in \mathbb{GL}(N, \mathbb{R}) | \mathbf{Q}^T \mathbf{Q} = \mathbf{Q} \mathbf{Q}^T = \mathbf{I}\}$ as

$$\underset{\mathbf{D} \in \mathbb{O}(N)}{\text{minimize}} \quad \frac{1}{L} \sum_{i=1}^L \text{Sp}(\mathbf{D}^T \mathbf{y}_i), \quad (2)$$

where $\text{Sp}(\cdot)$ is a sparsity-promoting function. This formulation is from the fact that if we have an orthogonal dictionary $\mathbf{D}^* \in \mathbb{O}(N)$, then $(\mathbf{D}^*)^T \mathbf{y}_i = (\mathbf{D}^*)^T \mathbf{D}^* \mathbf{x}_i = \mathbf{x}_i, \forall i$ are sparse. After obtaining the dictionary $\hat{\mathbf{D}}$ from solving problem (2), the sparse code can be obtained as $\{\mathbf{x}_i^* \approx (\hat{\mathbf{D}})^T \mathbf{y}_i\}_{i=1}^L$. Though solving problem (2) is still challenging due to the non-convex constraint, solutions with sample complexity and convergence analysis can be obtained by the high-dimensional probability and the non-convex optimization [1–5].

In this paper, we focus on the sparse coding problem by solving (2), since it enables more efficient solutions by only updating the dictionary at each iteration and has a stronger theoretical guarantee than the alternative optimization schemes. Ground-breaking works in this line of research [1–4] propose solutions to problem (2) via sequentially solving each atom of the dictionary, which leads to a long execution time. Recent works [5–7] have started to solve the entire dictionary together, which substantially reduces the execution time. However, these methods lead to degraded dictionary recovery performance with a finite number of samples. The main target of this paper is to develop an efficient sparse coding scheme, which facilitates fast implementation for superb dictionary recovery performance by a finite number of samples without atom-by-atom calculation.

1.1 Contributions

We consider sparse coding with an orthogonal dictionary and propose a two-stage sparse coding scheme, which hierarchically leverages the Riemannian geometry of the proposed two-stage optimization problem. In addition, we prove that if the proposed scheme is implemented over the sphere, with high probability, any one of the atoms in the true dictionary can be recovered exactly with finite data samples (up to a sign ambiguity). The proposed scheme facilitates fast and robust implementation on both synthetic and real-world data with superb dictionary recovery and data compression performances under a finite number of samples. The main contributions are summarized as follows.

- **Efficient Sparse Coding Scheme — Hierarchical Riemannian Pursuit:** We propose an efficient two-stage sparse coding scheme, named Hierarchical Riemannian Pursuit (HRP), via exploiting the global and local Riemannian geometry of the orthogonal group hierarchically. The proposed scheme facilitates fast implementation for superb dictionary recovery performance by a finite number of samples without atom-by-atom calculation. Specifically, in the first stage, we propose a non-convex ℓ_3 -norm maximization problem over the orthogonal group. This formulation enables an efficient parameter-free solver, namely the generalized power method (GPM). The first stage produces a result close to the target dictionary. In the second stage, we propose an efficient Riemannian projection gradient (RPG) method to solve a convex problem according to the local geometry of the orthogonal group. The second stage serves as the local refinement of the solution obtained at the first stage.
- **Exact Recovery Guarantee for One Atom:** To provide theoretical interpretation, we investigate the case where the proposed scheme is implemented over the sphere. Using high-dimensional

probability [28] and non-convex optimization [29] tools, we prove that, with high probability, the proposed scheme can exactly recover any of the atoms (up to a sign ambiguity) in the true dictionary with a finite number of samples.

- **Efficient on Real-World Sensor Data Compression:** We provide extensive experiments with both synthetic data and real-world data. The results verify the efficiency and robustness of our proposed scheme. For the synthetic data, the proposed scheme can achieve a superb dictionary recovery performance with a fast implementation under very broad conditions. A novel application of the wireless sensor data compression is first proposed in this work. The experiments on the real-world wireless sensor network (WSN) data show that the proposed scheme enjoys strong robustness to missing data and achieves a better root mean square error (RMSE) with one of the shortest execution time ($< 0.1s$) for the data compression task compared to the state-of-the-art baselines [1, 2, 4, 5, 18, 19, 21, 22].

1.2 Related Work

The recent success of non-convex optimization with high-dimensional signals indicates that the statistic properties of big data enable benign structures of non-convex problems and allows us to focus on average-case performance by excluding the worst-case instances in the general non-convex tasks [29]. Many important non-convex problems have proved to be solved efficiently, e.g., sparse coding (dictionary learning) [1–6, 27, 30], blind deconvolution [15, 31, 32], low-rank matrix recovery [33], phase retrieval [34, 35], matrix completion [36], learning shallow neural networks [37, 38], etc. Due to the scope, we discuss the closely related literature in the following.

The initial attempts using the non-convex approach to solve the sparse coding problem (2) focused on using ℓ_1 -norm or its approximation (e.g., *logcosh*) as the sparsity-promoting function [1–4]. However, these approaches result in a long execution time since one needs to break down problem (2) into solving N subproblems sequentially for an N -atom dictionary. To overcome this issue, [5, 6] proposed a novel *matching, stretching, and projection (MSP)* method to directly solve the problem (2) with $Sp(\cdot) = -\|\cdot\|_4^4$ over the orthogonal group. In [7], we generalized the result in [5, 6] to use $Sp(\cdot) = -\|\cdot\|_p^p$, $p > 2$, $p \in \mathbb{N}$, and showed that $p = 3$ achieves the lowest sample complexity among all $p > 2$, $p \in \mathbb{N}$. Compared to the atom-by-atom solutions [1–4], both methods [5–7] substantially reduce the execution time by directly recovering the entire dictionary with efficient parameter-free algorithms. However, these two methods can only recover an approximation of the target solution with finite data samples which degrades the recovery performance. In this paper, we propose an efficient two-stage scheme that exhibits a better performance than the schemes in [5–7] under a finite number of samples and inherits their efficiency.

Two-stage approaches are frequently adopted in recent non-convex optimization literature to obtain accurate results [1, 2, 32, 35, 39, 40]. Usually, the first stage will produce an approximation of the target solution, and the second stage refines the approximation to be more accurate. Specifically, for sparse coding, [1, 2] proposed a two-stage solution to exactly recover the dictionary, which solves a linear programming at the second stage. However, no efficient algorithm is provided in [1, 2] for the second stage. Qu et al. proposed a two-stage solution for the multichannel blind deconvolution problem [32] with an efficient algorithm to solve a similar linear programming in the second stage. However, directly adopting the second stage of [32] in the sparse coding problem will lead to sequentially solving the linear programming N times for an N -atom dictionary, which will incur a long execution time. In this paper, we propose an efficient two-stage sparse coding scheme to achieve a superb dictionary recovery performance without atom-by-atom calculation.

1.3 Paper Organization and Notations

The rest of the paper is organized as follows. Section 2 introduces the sparse coding problem and application examples. Section 3 presents the proposed two-stage sparse coding scheme. The theoretical results and the numerical experiments are demonstrated in Section 4 and Section 5, respectively. Finally, conclusions are drawn in Section 6.

In this paper, lowercase and uppercase bold face letters stand for column vectors and matrices, respectively. The i -th column vector in \mathbf{X} is $\mathbf{X}_{:,i}$. The vector \mathbf{d}_{-i} is \mathbf{d} with the i -th coordinate removed, and d_j denotes the j -th element of \mathbf{d} . $x_{i,j}$ is the j -th element of vector \mathbf{x}_i . $\mathbb{O}(N)$ and \mathbb{S}^{N-1} denote the N dimensional orthogonal group and the $N-1$ -sphere with real-valued entries, respectively. \mathbf{e}_i denotes the vector with a 1 in the i -th coordinate and 0's elsewhere. $(\cdot)^T$ and $\mathbb{E}[\cdot]$ denote the operations of transpose and expectation, respectively. $\|\cdot\|_p$ is the ℓ_p norm of a vector or the induced ℓ_p norm of a matrix.

For simplicity, the ℓ_2 norm of a vector is denoted by $\|\cdot\|$. \odot denotes the Hadamard product. $\langle \mathbf{X}, \mathbf{Y} \rangle$ is the general inner product of \mathbf{X} and \mathbf{Y} . $\mathcal{P}_{\mathbb{O}(N)}(\mathbf{D})$ projects \mathbf{D} onto the orthogonal group. $\nabla f(\mathbf{x})$ and $\nabla_{grad} f(\mathbf{x})$ are the sub-gradient and the Riemannian sub-gradient of $f(\cdot)$ with respect to \mathbf{x} . For a positive integer N , define $[N] = \{1, 2, \dots, N\}$. The set $\{\mathbf{x}_i, i \in [N]\}$ is abbreviated as $\{\mathbf{x}_i\}_{i=1}^N$. $\lfloor \cdot \rfloor$ and $\lceil \cdot \rceil$ denote the floor operator and taking the abstract value, respectively. $\mathbf{x} \sim^{i.i.d} \mathcal{BG}(\theta)$ represents that vector \mathbf{x} has i.i.d elements and each is a product of independent Bernoulli and standard normal random variables: $x_i = b_i g_i$, where $b_i \sim \text{Ber}(\theta)$ and $g_i \sim \mathcal{N}(0, 1)$.

2 Sparse Coding Problem and Application Examples

2.1 Sparse Coding Problem

In this section, we shall illustrate the sparse coding problem. We consider that the data samples $\{\mathbf{y}_i\}_{i=1}^L$ are collected by the sparse coding processor with $\mathbf{y}_i \in \mathbb{R}^N$, and $L > N$. Each sample is assumed to be generated by

$$\mathbf{y}_i = \mathbf{D}^* \mathbf{x}_i^*, \forall i = 1, \dots, L, \quad (3)$$

where \mathbf{D}^* is the orthogonal dictionary and \mathbf{x}_i is the sparse code. The orthogonality assumption enables efficient implementation to solve the sparse coding problem, as we will illustrate in the following sections. The goals of the sparse coding are:

- to learn the orthogonal dictionary $\mathbf{D}^* \in \mathbb{O}(N)$ from the given data set $\{\mathbf{y}_i\}_{i=1}^L$,
- and to find the sparse code \mathbf{x}_i^* such that $\mathbf{y}_i = \mathbf{D}^* \mathbf{x}_i^*$.

One can achieve the above goals by alternately updating the dictionary and the sparse code. However, we consider separating the two by first learning the dictionary and then the sparse code since this is more computationally efficient. This separate learning can be done by optimizing the generic non-convex problem (2). The optimizer returns a learned dictionary, and a simple matrix-vector multiplication can return the sparse code.

2.2 Application Examples

In this section, we give two important application examples that involve solving the sparse coding problem.

Example 1 (Data Compression in Industrial IoT (IIoT) Networks): Consider a dense IIoT network, where a total number of N geographically distributed IIoT sensors jointly monitor a dynamic plant. At the i -th time slot, the IIoT sensors transmit their local plant state measurements $\mathbf{y}_i \in \mathbb{R}^N$ to a data center (DC), which relays the sensor data to a remote controller to form closed-loop industrial control. Due to the spatial and temporal correlation of the IIoT sensors, the collection of the sensor data in L time slots $\{\mathbf{y}_i\}_{i=1}^L$ has a sparse representation $\mathbf{y}_i = \mathbf{D}^* \mathbf{x}_i^*, \forall i = 1, \dots, L$. To reduce the communication cost, the DC can first compress the sensor data by performing the sparse coding over the historical samples $\{\mathbf{y}_i\}_{i=1}^L$, it then transmits the learned dictionary $\hat{\mathbf{D}}$ and the sparse codes $\{\hat{\mathbf{x}}_i\}_{i=1}^L$ to the remote controller.

Example 2 (Image Denoising): For image denoising application [10, 41], the noisy training data samples $\{\tilde{\mathbf{y}}_i\}_{i=1}^L$ are obtained by vectorizing a total number of L randomly sampled $\sqrt{N} \times \sqrt{N}$ -sized image patches from the noisy image. Due to the correlation among image patches, the i -th patch of the clean image can be represented by $\mathbf{y}_i = \mathbf{D}^* \mathbf{x}_i^*$, where \mathbf{D}^* is the dictionary containing the compact features of the whole image, and \mathbf{x}_i^* is the sparse code for the i -th patch. Applying the sparse coding to the noisy training samples $\{\tilde{\mathbf{y}}_i\}_{i=1}^L$, the de-noised image can be reconstructed using the de-noised image patches $\{\hat{\mathbf{D}} \hat{\mathbf{x}}_i\}_{i=1}^L$ by averaging the overlapping pixels, where $\hat{\mathbf{D}}$ and $\{\hat{\mathbf{x}}_i\}_{i=1}^L$ are the learned dictionary and the sparse codes, respectively.

3 Proposed Hierarchical Riemannian Pursuit Sparse Coding

In this section, we shall present the proposed HRP scheme for sparse coding, for which the signal processing flow is summarized in Fig. 1.

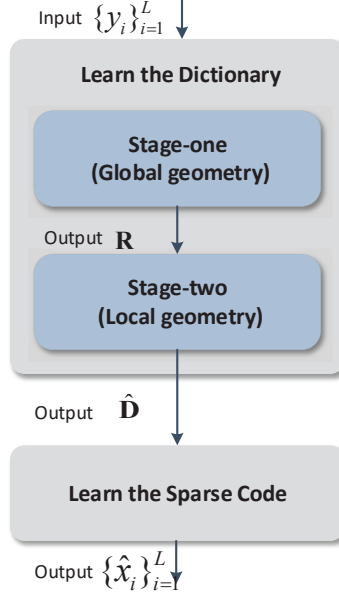


Figure 1: Signal processing flow for the proposed HRP sparse coding scheme.

3.1 Learn the Dictionary

We start from the elaboration of the two-stage dictionary learning.

3.1.1 Stage One

At Stage One, we propose to solve

$$\mathcal{P}_1 : \underset{D \in \mathbb{O}(N)}{\text{minimize}} \quad -\frac{1}{L} \sum_{i=1}^L \|D^T y_i\|_3^3, \quad (4)$$

where $-\|\cdot\|_3^3$ is a differentiable, non-smooth, and concave sparsity-promoting function. The choice of the objective function is inspired by the recent result that maximizing the p -the power of the ℓ_p -norm ($p > 2$, $p \in \mathbb{N}$) with the unit ℓ_2 -norm constraint leads to sparse (or spiky) solutions [5–7, 30, 42]. An illustration of this is given in Fig. 2. In this paper, we use $p = 3$, i.e., minimizing $-\|\cdot\|_3^3$ in Problem (4), which has several benefits. First, the differentiable and concavity of this function, together with the global geometry of the orthogonal group enables a fast and parameter-free algorithm. Second, as we have proved in [7], the sample complexity for consistency achieves the minimum when $p = 3$, among all the choices of p ($p > 2$, $p \in \mathbb{N}$) for maximizing the ℓ_p -norm over the orthogonal group.

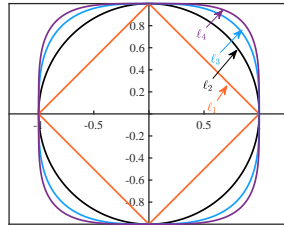


Figure 2: Unit spheres of the ℓ_p in \mathbb{R}^2 , where $p = 1, 2, 3, 4$. The sparsest points on the unit ℓ_2 -sphere, e.g., points $(0, 1)$, $(0, -1)$, $(1, 0)$ and $(-1, 0)$ in \mathbb{R}^2 , have the largest ℓ_p -norm ($p > 2$, $p \in \mathbb{N}$).

Stage One aims at minimizing a concave function, $-\|\cdot\|_3^3$, over a compact Riemannian manifold, $\mathbb{O}(N)$. Such a problem can be solved by plenty of optimization methods on the Riemannian manifold, e.g., Riemannian gradient descent and Riemannian trust region. However, since the orthogonal group is a compact set in the vector space, the more efficient GPM [43] can be applied. In each iteration, the

GPM minimizes a linear surrogate of the concave objective function over the constraint compact set. Specifically, using GPM to solve the generic problem

$$\min_{x \in Q} \underbrace{f(x)}_{\text{Concave}},$$

we have the following iteration:

$$\mathbf{x}^{t+1} = \underset{\mathbf{s} \in Q}{\operatorname{argmin}} f(\mathbf{x}^{(t)}) + \langle \mathbf{s} - \mathbf{x}^{(t)}, \nabla f(\mathbf{x}^{(t)}) \rangle, \quad (5)$$

where Q is a compact set and $\nabla f(\mathbf{x})$ is any subgradient of f at \mathbf{x} . Applying GMP to solve Problem \mathcal{P}_1 , at the t_1 -th iteration, we have

$$\mathbf{D}^{(t_1+1)} = \operatorname{Polar}\left(-\nabla \frac{1}{L} \sum_{i=1}^L \|(\mathbf{D}^{(t_1)})^T \mathbf{y}_i\|_3^3\right). \quad (6)$$

We have

$$\begin{aligned} & -\nabla \frac{1}{L} \sum_{i=1}^L \|(\mathbf{D}^{(t_1)})^T \mathbf{y}_i\|_3^3 \\ &= -\frac{1}{L} \mathbf{Y} (|(\mathbf{D}^{(t_1)})^T \mathbf{Y}| \odot (\mathbf{D}^{(t_1)})^T \mathbf{Y})^T, \end{aligned} \quad (7)$$

where $\mathbf{Y} = [\mathbf{y}_1, \mathbf{y}_2, \dots, \mathbf{y}_L] \in \mathbb{R}^{N \times L}$. $\operatorname{Polar}(\cdot)$ is the polar decomposition of a matrix, and (6) is obtained by the following proposition.

Proposition 1. *Let $\mathbf{C} \in \mathbb{R}^{N \times N}$, and the singular values of \mathbf{C} are denoted by $\sigma_i(\mathbf{C}), i = 1, \dots, N$. Then, we have*

$$\max_{\mathbf{s} \in \mathbb{O}(N)} \langle \mathbf{s}, \mathbf{C} \rangle = \sum_{i=1}^N \sigma_i(\mathbf{C})$$

with maximizer $\mathbf{s} = \operatorname{Polar}(\mathbf{C})$.

Proof. The proof can be done by changing the compact set from the Stiefel manifold to the orthogonal group in the proof of [43, Proposition 7]. \square

To obtain a more accurate dictionary recovery result, we propose the following Stage Two to refine the solution of Stage One.

3.1.2 Stage Two

At Stage Two, we propose to solve

$$\begin{aligned} \mathcal{P}_2: \quad & \underset{\mathbf{D}}{\operatorname{minimize}} \quad \frac{1}{L} \sum_{i=1}^L |\mathbf{D}^T \mathbf{y}_i|, \\ & \text{subject to} \quad \mathbf{D}^T \mathbf{R} + \mathbf{D} \mathbf{R}^T = 2\mathbf{I}, \end{aligned} \quad (8)$$

where \mathbf{R} is the solution obtained at Stage One. The equality constraint is developed from the first-order expansion of the orthogonal group at \mathbf{R} . This constraint can be regarded as a convex relaxation of the orthogonal constraint at the neighborhood of the target dictionary. The relaxed convex constraint and the objective function make this problem convex and enable efficient local search, which can refine the coarse solution in Stage One under finite data samples. Therefore, we can expect to obtain a more accurate result by solving Problem \mathcal{P}_2 with simple algorithms, after solving Problem \mathcal{P}_1 .

Problem \mathcal{P}_2 is a convex problem, which can be solved by existing convex solvers. However, the implementation can be relatively slow. In this paper, inspired by the rounding technique in [32] for the multi-channel blind deconvolution problem, we propose an efficient RPG to solve Problem \mathcal{P}_2 . The algorithm is derived based on the fact that the moving direction from \mathbf{R} to the solution of Problem \mathcal{P}_2 is on the tangent space of the orthogonal group at \mathbf{R} , which is characterized in the following Lemma 1.

Lemma 1. Let $\mathbf{X} \in \mathbb{O}(N)$ and $\mathbf{Z} \in \mathbb{R}^{N \times N}$. Then $\mathbf{Z}^T \mathbf{X} + \mathbf{Z} \mathbf{X}^T = 2\mathbf{I}$ if and only if

$$\Delta = \mathbf{Z} - \mathbf{X} \in \mathbf{X} \mathcal{S}_{skew}(N),$$

where $\mathcal{S}_{skew}(N)$ denotes the set of all skew-symmetric $N \times N$ matrices. $\mathbf{X} \mathcal{S}_{skew}(N)$ is the tangent space to an orthogonal group at \mathbf{X} .

Proof. See Appendix B. \square

Given that the moving direction is on the tangent space of the orthogonal group at \mathbf{R} , the RPG at the t_2 -th iteration, iterates as

$$\mathbf{D}^{(t_2+1)} = \mathbf{D}^{(t_2)} - \tau \mathcal{P}_{\mathbf{R}^\perp} \left(\nabla \frac{1}{L} \sum_{i=1}^L |(\mathbf{D}^{(t_2)})^T \mathbf{y}_i| \right), \quad (9)$$

where

$$\nabla \frac{1}{L} \sum_{i=1}^L |(\mathbf{D}^{(t_2)})^T \mathbf{y}_i| = \frac{1}{L} \mathbf{Y} \text{sign}((\mathbf{D}^{(t_2)})^T \mathbf{Y})^T, \quad (10)$$

and

$$\mathcal{P}_{\mathbf{R}^\perp}(\mathbf{A}) = \frac{1}{2}(\mathbf{A} - \mathbf{R} \mathbf{A}^T \mathbf{R}), \quad (11)$$

which projects \mathbf{A} onto the tangent space of \mathbf{R} over the orthogonal group [44]. Since the orthogonal constraint is relaxed, an orthogonal projection, $\mathcal{P}_{\mathbb{O}(N)}(\cdot)$, is necessary after Stage Two.

To summarize, we show an example to illustrate the proposed two-stage dictionary learning in Fig. 3.

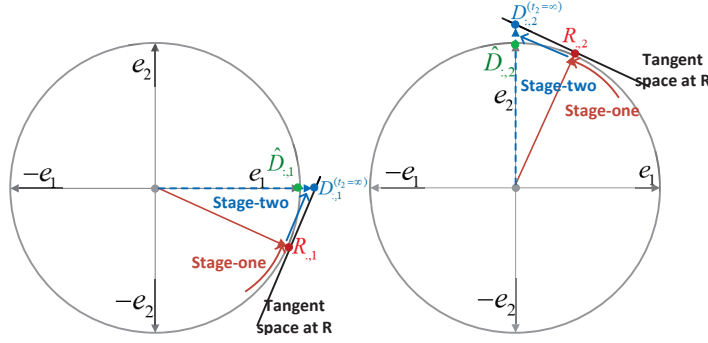


Figure 3: An example to illustrate the two-stage scheme. Assume that the target orthogonal dictionary is $\mathbf{D}^* = \begin{bmatrix} 1 & 0 \\ 0 & 1 \end{bmatrix}$, then the target solution for each column is \mathbf{e}_1 and \mathbf{e}_2 . The left subfigure shows the behavior of the first column. Specifically, at the first stage, the scheme searches along the manifold to find a point $\mathbf{R}_{:,1}$ that is very closed to \mathbf{e}_1 . Then, at the second stage, the scheme searches along the tangent space of $\mathbf{R}_{:,1}$ to obtain $\mathbf{D}_{:,1}^{(t_2=\infty)}$, which is a scaled version of \mathbf{e}_1 . Therefore, the final result $\hat{\mathbf{D}}_{:,1}$ can be obtained by a projection (or normalization). Similarly, the right subfigure shows the behavior of the second column with the target solution, \mathbf{e}_2 .

3.2 Learn the Sparse Code

Based on the learned dictionary $\hat{\mathbf{D}}$, the estimate of the sparse code can be obtained directly by $\hat{\mathbf{x}}_i = \hat{\mathbf{D}}^T \mathbf{y}_i, \forall i$. However, some applications have strict sparsity requirements of $\hat{\mathbf{x}}_i$, e.g., data compression. In this case, one can obtain the sparse code by solving

$$\begin{aligned} & \underset{\{\mathbf{x}_i\}_{i=1}^L}{\text{minimize}} && \sum_{i=1}^L \|\hat{\mathbf{D}}^T \mathbf{y}_i - \mathbf{x}_i\|^2 \\ & \text{subject to} && \|\mathbf{x}_i\|_0 \leq T_0, \forall i, \end{aligned} \quad (12)$$

where T_0 is the required number of non-zero elements in \mathbf{x}_i . Problem (12) has the well-known hard thresholding solution, $\tilde{\mathbf{x}}_i = \mathcal{T}_{T_0}(\hat{\mathbf{D}}^T \mathbf{y}_i)$ [18], where $\mathcal{T}_{T_0}(\mathbf{a})$ selects T_0 elements in \mathbf{a} with the largest ℓ_2 -norm and sets the other elements to zero.

To summarize, the solution for the proposed sparse representation scheme is given in Algorithm 1.

Algorithm 1 Proposed HRP Sparse Coding

Require: $\{\mathbf{y}_i\}_{i=1}^L$

```

1: Learn the Dictionary
2: Solve Problem  $\mathcal{P}_1$  by GPM
3: Initialization: random  $\mathbf{D}^{(0)} \in \mathbb{O}(N)$ ,  $t_1 = 0$ .
4: while not converge do
5:    $\mathbf{D}^{(t_1+1)} = \text{Polar}(-\nabla \frac{1}{L} \sum_{i=1}^L \|(\mathbf{D}^{(t_1)})^T \mathbf{y}_i\|_3^3)$ 
6:    $t_1 = t_1 + 1$ 
7: end while
8: Solve Problem  $\mathcal{P}_2$  by RPG
9:  $\mathbf{R} = \mathbf{D}^{(t_1)}$ ,  $t_2 = 0$ 
10: while not converge do
11:    $\mathbf{D}^{(t_2+1)} = \mathbf{D}^{(t_2)} - \tau \mathcal{P}_{\mathbf{R}^\perp}(\nabla \frac{1}{L} \sum_{i=1}^L |(\mathbf{D}^{(t_2)})^T \mathbf{y}_i|)$ 
12:    $t_2 = t_2 + 1$ 
13: end while
14:  $\hat{\mathbf{D}} = \mathcal{P}_{\mathbb{O}(N)}(\mathbf{D}^{(t_2)})$ .
15: Learn the Sparse Code
16:  $\hat{\mathbf{x}}_i = \hat{\mathbf{D}}^T \mathbf{y}_i, \forall i$  or  $\hat{\mathbf{x}}_i = \mathcal{T}_{T_0}(\hat{\mathbf{D}}^T \mathbf{y}_i), \forall i$ .

```

4 Exact Recovery of One Atom

Since the dictionary learning contains most of the technical challenges in the proposed sparse coding scheme, rigorous interpretation needs to be presented to justify its correctness. In this section, we investigate why and how the dictionary learning in the proposed scheme can achieve a superb dictionary recovery performance with a finite number of samples. Unfortunately, the exact analysis over the orthogonal group is extremely difficult. In fact, even whether a local optimum of the orthogonal dictionary learning problem (2) exists is still a mathematically open problem as pointed out in [5]. Through extensive numerical simulations, we find that the convergence behaviors of the proposed scheme over the orthogonal group and over the sphere are very similar, as shown in Fig. 4. Moreover, inspired by the pioneer works in [1–4] that learn the orthogonal dictionary over the sphere, we therefore seek for a relaxation to prove that our proposed scheme can exactly recovery any atom (up to a sign ambiguity) of the dictionary with a finite number of samples when it is applied over the sphere. The analysis is highly non-trivial due to the non-convexity in the proposed scheme and the randomness in the data samples.

Considering the recovery of one atom of the orthogonal dictionary, the dictionary learning in the proposed scheme is specialized as follows:

- **Stage One:** solves the optimization problem

$$\hat{\mathcal{P}}_1 : \underset{\mathbf{d} \in \mathbb{S}^{N-1}}{\text{minimize}} \quad -\frac{1}{L} \sum_{i=1}^L \|\mathbf{d}^T \mathbf{y}_i\|_3^3 \quad (13)$$

by GPM:

$$\mathbf{d}^{(t_1+1)} = \text{Polar}(-\nabla \frac{1}{L} \sum_{i=1}^L \|(\mathbf{d}^{(t_1)})^T \mathbf{y}_i\|_3^3), \quad (14)$$

where the variable \mathbf{d} is constrained on a unit sphere as it is an estimate of one column in the orthogonal dictionary.

- **Stage Two:** solves the optimization problem

$$\begin{aligned} \hat{\mathcal{P}}_2 : \underset{\mathbf{d}}{\text{minimize}} \quad & \frac{1}{L} \sum_{i=1}^L |\mathbf{d}^T \mathbf{y}_i|. \\ \text{subject to} \quad & \mathbf{d}^T \mathbf{r} = 1 \end{aligned} \quad (15)$$

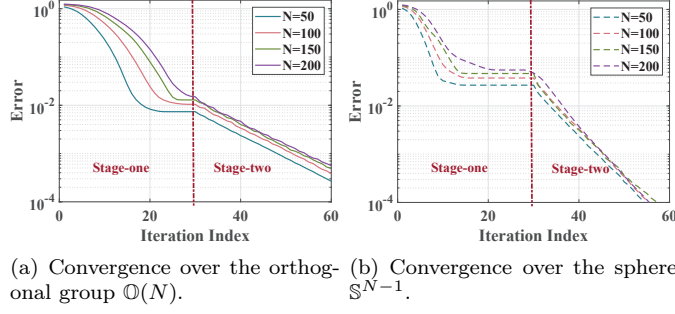


Figure 4: Convergence comparison on the orthogonal group and the sphere. In each trial, we generated the received data by $\{\mathbf{y}_i\}_{i=1}^{10^5} = \mathbf{D}^* \{\mathbf{x}_i^*\}_{i=1}^{10^5}$, where the dictionary $\mathbf{D}^* \in \mathbb{R}^{N \times N}$ is a random orthogonal matrix via QR decomposition of a random matrix with elements uniformly distributed in the interval $(0, 1)$ in an i.i.d manner. The sparse code $\{\mathbf{x}_i^*\}_{i=1}^{10^5}$ satisfies $\mathbf{x}_i^* \in \mathbb{R}^N \sim^{i.i.d} \mathcal{BG}(0.1)$. The initial point of the proposed scheme over the sphere is generated uniformly randomly over the sphere and the initial point of the proposed scheme over the orthogonal group is generated via QR decomposition of a random matrix with elements following the normal distribution in an i.i.d manner. For $\mathbb{O}(N)$ we have Error = $\sqrt{\min_{\mathbf{J} \in \mathcal{J}} \frac{\|\hat{\mathbf{D}} - \mathbf{D}^* \mathbf{J}\|_F^2}{\|\mathbf{D}^* \mathbf{J}\|_F^2}}$, where \mathcal{J} is the set contains all the N-dimensional sign-permutation matrices. For \mathbb{S}^{N-1} , we have Error = $\sqrt{\min_{\mathbf{e} \in \mathcal{E}} \frac{\|\hat{\mathbf{d}} - \mathbf{D}^* \mathbf{e}\|_F^2}{\|\mathbf{D}^* \mathbf{e}\|_F^2}}$, where $\mathcal{E} = \{\pm \mathbf{e}_n, n \in [N]\}$.

by RPG:

$$\mathbf{d}^{(t_2+1)} = \mathbf{d}^{(t_2)} - \mathcal{P}_{\mathbf{r}, \perp}(\tau^{(t_2)} \nabla \frac{1}{L} \sum_{i=1}^L |(\mathbf{d}^{(t_2)})^T \mathbf{y}_i|), \quad (16)$$

where \mathbf{r} is the result from Stage One (14), and $\mathcal{P}_{\mathbf{r}, \perp}(\cdot)$ is a projection onto the tangent space of \mathbf{r} over the sphere. The final estimate is $\hat{\mathbf{d}} = \frac{\mathbf{d}^{(t_2)}}{\|\mathbf{d}^{(t_2)}\|}$, where $\mathbf{d}^{(t_2)}$ is the result from Stage Two.

There is an intrinsic ambiguity in recovering one atom in the dictionary due to the bilinear nature of the sparse coding, namely the *sign ambiguity* [1, 2, 4]. Hence, we consider that one atom is exactly recovered if the estimate equals that atom up to a sign ambiguity, i.e., $\hat{\mathbf{d}}$ is said to exactly recover one atom in the true dictionary if $\hat{\mathbf{d}} = \mathbf{d}^*$ with $\mathbf{d}^* \in \{\pm \mathbf{D}_{:,1}^*, \pm \mathbf{D}_{:,2}^*, \dots, \pm \mathbf{D}_{:,N}^*\}$. In the following, we show that with finite data samples, Stage One of the proposed dictionary learning can obtain a solution very close to one of the atoms in the true dictionary (up to a sign ambiguity), and Stage Two can successfully refine the solution to be exactly the ground truth atom (up to a sign ambiguity). Without loss of generality, we have the following assumptions in the remaining theoretical analysis.

- We assume $\mathbf{D}^* = \mathbf{I}$ since the problem is invariant to rotations, i.e., orthogonal transformation has no impact on the analysis [4]. Hence, we have any of the true atoms \mathbf{d}^* satisfying $\mathbf{d}^* \in \{\pm \mathbf{e}_1, \pm \mathbf{e}_2, \dots, \pm \mathbf{e}_N\}$.
- We assume that each element in the sparse code $\mathbf{x}_i^* \in \mathbb{R}^N$ is i.i.d. Bernoulli-Gaussian, i.e., $x_{i,j}^* \sim^{i.i.d} \mathcal{BG}(\theta)$, which is a reasonable model for generic sparse coefficients [1–7].

4.1 Approximate Recovery at Stage One

To bring more insight, we first show the reason why non-convex Problem $\hat{\mathcal{P}}_1$ is tractable by the high-dimensional geometry for the instance of Problem $\hat{\mathcal{P}}_1$ illustrated in Fig. 5. The figure shows that as the number of samples L grows large, Problem $\hat{\mathcal{P}}_1$ tends to have a benign geometry in the sense that it has no spurious local minimizers, and every local optimum is very close to one of the target atoms up to a sign ambiguity. These geometric properties are the key for a first-order method to find an estimated global solution for a non-convex problem. In the following, we will show that the properties observed from the toy example in Fig. 5 hold true with mathematical proof.

4.1.1 Statistical Analysis

We first show that Problem $\hat{\mathcal{P}}_1$ concentrates to the population problem, i.e., the objective in $\hat{\mathcal{P}}_1$ becomes $\mathbb{E}[-\frac{1}{L} \sum_{i=1}^L \|\mathbf{d}^T \mathbf{y}_i\|_3^3]$, when the sample size is large enough with the following lemma.

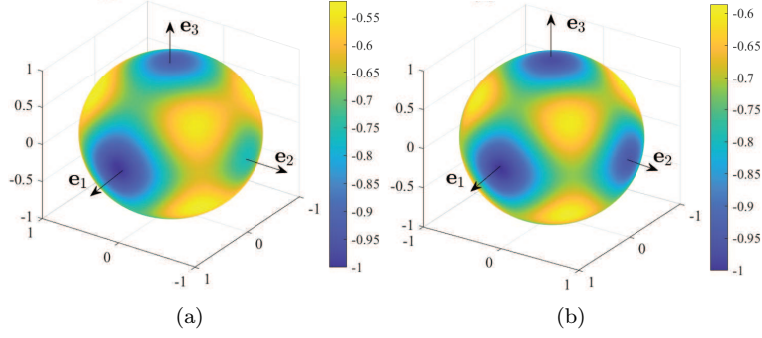


Figure 5: High-dimensional geometry of Problem (13) with $\mathbf{x}_i \in \mathbb{R}^3, \mathbf{x}_i \sim^{i.i.d} \mathcal{BG}(\theta)$ with $\theta = 0.2$, $\mathbf{y}_i = \mathbf{D}^* \mathbf{x}_i^*, \forall i$, $\mathbf{D}^* = \begin{bmatrix} 1 & 0 & 0 \\ 0 & 1 & 0 \\ 0 & 0 & 1 \end{bmatrix}$, and $\mathbf{d} \in \mathbb{S}^2$ as the sample size grows from (a) $L = 1000$ to (b) $L = 100000$.

Lemma 2. (*Concentration Property*) Let $\mathbf{x}_i \in \mathbb{R}^N, \mathbf{x}_i \sim^{i.i.d} \mathcal{BG}(\theta)$ with $\theta \in (\frac{1}{N}, \frac{1}{2})$, $\mathbf{D}^* = \mathbf{I}$, $\mathbf{y}_i = \mathbf{D}^* \mathbf{x}_i^*, \forall i$, and $f(\mathbf{d}) = -\frac{1}{L} \sum_{i=1}^L \|\mathbf{d}^T \mathbf{y}_i\|_3^3$. There exist positive constants c_1 and C_1 , for any $\delta \in (0, c_1/(N \log(L) \log(NL)\theta^{\frac{1}{3}})^{3/2})$ and $L \geq C_1 \delta^{-2} N \theta \log(\frac{N\theta}{\delta})$, such that

$$\begin{aligned} \Pr \left[\sup_{\mathbf{d} \in \mathbb{S}^{N-1}} \|f(\mathbf{d}) - \mathbb{E}[f(\mathbf{d})]\| \leq \delta \right] &\geq 1 - L^{-1}, \\ \Pr \left[\sup_{\mathbf{d} \in \mathbb{S}^{N-1}} \|\nabla_{grad} f(\mathbf{d}) - \nabla_{grad} \mathbb{E}[f(\mathbf{d})]\| \leq \delta \right] &\geq 1 - L^{-1}, \end{aligned}$$

where $\nabla_{grad} f(\mathbf{d})$ is the Riemannian gradient of $f(\mathbf{d})$ at \mathbf{d} .

Proof. See Appendix C. □

4.1.2 Landscape Analysis of the ℓ_3 -norm Objective over the Sphere

Lemma 2 inspires us to first investigate the geometry for the population problem since optimizing a deterministic problem is easier to analyze. The stationary points of the population problem are characterized in the following Lemma 3.

Lemma 3. (*Isolated Stationary Points of the Population Problem*) Let $\mathbf{x}_i \in \mathbb{R}^N \sim^{i.i.d} \mathcal{BG}(\theta)$ with $\theta \in (\frac{1}{N}, \frac{1}{2})$, $\mathbf{y}_i = \mathbf{D}^* \mathbf{x}_i^*, \forall i$, with $\mathbf{D}^* = \mathbf{I}$, and $f(\mathbf{d}) = -\frac{1}{L} \sum_{i=1}^L \|\mathbf{d}^T \mathbf{y}_i\|_3^3$. We have

$$\nabla_{grad} \mathbb{E}[f(\mathbf{d})] = \mathbf{0} \tag{17}$$

if and only if $\mathbf{d} \in \mathcal{S}'$ with

$$\mathcal{S}' = \left\{ \frac{1}{\sqrt{k}} \mathbf{d} : \mathbf{d} \in \{-1, 0, 1\}^N, \|\mathbf{d}\|_0 = k, k \in [N] \right\}. \tag{18}$$

Specifically, $k = 1$ corresponds to the $2N$ global optimum $\mathbf{d}^* \in \{\pm \mathbf{e}_1, \pm \mathbf{e}_2, \dots, \pm \mathbf{e}_N\}$.

Proof. See Appendix D. □

Lemma 3 shows that at a population level, the stationary points are isolated and there are $2N$ equivalent global minimizers that have a symmetric property. These results motivate us to partition the whole \mathbb{S}^{N-1} into $2N$ symmetric regions, and consider $2N$ (disjoint) subsets of each region [4, 32]. We define these subsets as *good subsets*:

Definition 1. (*Good Subsets*) For any $\zeta \in (0, \infty)$ and $n \in [N]$, the good subsets are defined as

$$\begin{aligned} \mathcal{S}_\zeta^{(n+)} &\doteq \left\{ \mathbf{d} \in \mathbb{S}^{N-1} : d_n > 0, \frac{d_n^2}{\|\mathbf{d}_{-n}\|_\infty^2} \geq 1 + \zeta \right\}, \\ \mathcal{S}_\zeta^{(n-)} &\doteq \left\{ \mathbf{d} \in \mathbb{S}^{N-1} : d_n < 0, \frac{d_n^2}{\|\mathbf{d}_{-n}\|_\infty^2} \geq 1 + \zeta \right\}. \end{aligned} \tag{19}$$

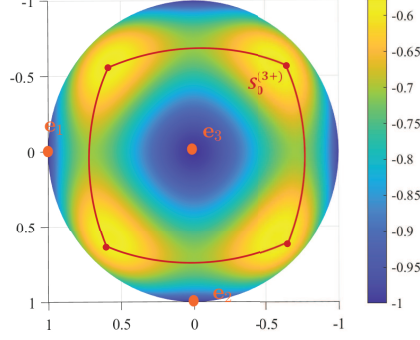


Figure 6: Top view of an example subsets $\mathcal{S}_0^{(3+)}$ for $N = 3$ of the partition in Definition 1.

Fig. 6 shows an example of subset $\mathcal{S}_0^{(3+)}$ for $N = 3$. The above partition of the sphere ensures that, for the population problem, there are no stationary points other than the $2N$ global minimizers in the good subsets, and there is only one optimal point within each $\{\mathcal{S}_\zeta^{(n\pm)} \mid \forall n \in [N]\}$. Furthermore, the points in $\mathcal{S}_\zeta^{(n+)}$ are closer to \mathbf{e}_n than all the other $2N - 1$ optimal points. If the algorithm initialized in this region finally converges to an approximation of \mathbf{e}_n rather than the other optimal solutions, then the results will automatically carry over to all the other $2N - 1$ subsets by the symmetry of \mathbb{S}^{N-1} . To formalize the above insights, we first characterize the benign geometry for the population problem in the following lemma.

Lemma 4. (*Benign Global Geometry for the Population Problem*) Under the conditions of Lemma 3, with any $\zeta_0 \in (0, 1)$, the below statement holds simultaneously for all the $2N$ subsets $\{\mathcal{S}_{\zeta_0}^{(n\pm)}, \forall n \in [N]\}$ (stated only for $\mathcal{S}_{\zeta_0}^{(N+)}$): For all $\mathbf{d} \in \mathcal{S}_{\zeta_0}^{(N+)}$ and all $n' \in [N], n' \neq N$ with $d_{n'} \neq 0$, we have

$$\langle -\nabla_{\text{grad}} \mathbb{E}[f(\mathbf{d})], \frac{1}{d_N} \mathbf{e}_N - \frac{1}{d_{n'}} \mathbf{e}_{n'} \rangle \geq \frac{3\sqrt{2\pi}}{N} \theta(1 - \theta) \frac{\zeta_0}{1 + \zeta_0}. \quad (20)$$

Proof. See Appendix E. □

Lemma 4 shows that for all points in $\mathcal{S}_{\zeta_0}^{(N+)}$, the negative Riemannian gradient of the population objective points towards the target solution \mathbf{e}_N coordinate-wisely. Leveraging the concentration property in Lemma 2, we further show in the following Lemma 5 a similar result on the *benign global geometry* of the empirical Problem $\hat{\mathcal{P}}_1$.

Lemma 5. (*Benign Global Geometry for the Empirical Problem*) Under the conditions of Lemma 2, there exist positive constants c_1 and C_1 for any $\delta \in (0, c_1/(N \log(L) \log(NL)\theta^{\frac{1}{3}})^{3/2})$ and $\zeta_0 \in (0, 1)$. When $L \geq C_1 \delta^{-2} N \theta \log(\frac{N\theta}{\delta})$, the below statement holds simultaneously with a probability of at least $1 - L^{-1}$ for all the $2N$ subsets $\{\mathcal{S}_{\zeta_0}^{(n\pm)}, \forall n \in [N]\}$ (stated only for $\mathcal{S}_{\zeta_0}^{(N+)}$): For all $\mathbf{d} \in \mathcal{S}_{\zeta_0}^{(N+)}$ and all $n' \in [N], n' \neq N$ with $d_{n'} \neq 0$, we have

$$\begin{aligned} & \langle -\nabla_{\text{grad}} f(\mathbf{d}), \frac{1}{d_N} \mathbf{e}_N - \frac{1}{d_{n'}} \mathbf{e}_{n'} \rangle \\ & \geq \frac{3\sqrt{2\pi}}{N} \theta(1 - \theta) \frac{\zeta_0}{1 + \zeta_0} - \underbrace{\delta \left\| \frac{1}{d_{n'}} \mathbf{e}_{n'} - \frac{1}{d_N} \mathbf{e}_N \right\|}_{\text{trade-off term}}. \end{aligned} \quad (21)$$

Proof. See Appendix F. □

Remark 1. (*Trade-off between Sample Complexity and Recovery Accuracy*) From Lemma 5, we know that, with $L \rightarrow \infty, \delta \rightarrow 0$ and for all points in $\mathcal{S}_{\zeta_0}^{(N+)}$, the negative Riemannian gradient points towards the target solution \mathbf{e}_N coordinate-wisely, while with finite L , this benign geometry holds only when $\frac{3\sqrt{2\pi}}{N} \theta(1 + \theta) \frac{\zeta_0}{1 + \zeta_0} > \delta \left\| \frac{1}{d_{n'}} \mathbf{e}_{n'} - \frac{1}{d_N} \mathbf{e}_N \right\|$ with high probability. However, when L is large enough, with high probability, the benign geometry can hold in a large fraction of $\mathcal{S}_{\zeta_0}^{(N+)}$, except an area that is very close to the target solution ($\left\| \frac{1}{d_{n'}} \mathbf{e}_{n'} - \frac{1}{d_N} \mathbf{e}_N \right\|$ is very large). This means that with a sufficiently large number of samples,

the possible stationary points of Problem $\hat{\mathcal{P}}_1$ fall in the region that is very close to the target with high probability.

4.1.3 Convergence Analysis of the GPM

Then, we will show the convergence properties of GPM in the following lemma.

Lemma 6. (Convergence of GPM to the Stationary Point in the Initialized Good Set) Let $\mathbf{x}_i \in \mathbb{R}^N$, $\mathbf{x}_i \sim i.i.d \mathcal{BG}(\theta)$ with $\theta \in (\frac{1}{N}, \frac{1}{12}\sqrt{\frac{\pi}{2}})$, $\mathbf{D}^* = \mathbf{I}$, $\mathbf{y}_i = \mathbf{D}^* \mathbf{x}_i^*$, $\forall i$, and $f(\mathbf{d}) = -\frac{1}{L} \sum_{i=1}^L \|\mathbf{d}^T \mathbf{y}_i\|_3^3$. There exist some positive constants c_2 and C_2 , for any $\delta \in (0, c_2/(N \log(L) \log(NL)\theta^{\frac{1}{3}})^{3/2})$ and $\zeta_0 \in (0, 1)$. Whenever $L \geq C_2 \delta^{-2} N \theta \log(\frac{N\theta}{\delta})$, the below statement holds simultaneously with high probability for all the $2N$ subsets $\{\mathcal{S}_{\zeta_0}^{(n\pm)}, \forall n \in [N]\}$ (stated only for $\mathcal{S}_{\zeta_0}^{(N+)}$): When $\mathbf{d}^{(0)} \in \mathcal{S}_{\zeta_0}^{(N+)}$, we have the iterates $\mathbf{d}^{(t_1)}$, $t_1 = 1, 2, \dots$, generated by the GPM in (14) stay in $\mathcal{S}_{\zeta_0}^{(N+)}$ and

$$\nabla_{grad} f(\mathbf{r}) = \mathbf{0}, \quad (22)$$

where $\mathbf{r} = \lim_{t_1 \rightarrow \infty} \mathbf{d}^{(t_1)}$.

Proof. See Appendix G. □

4.1.4 Summary of Stage One

The benign geometry in Lemma 5 and the convergence of the GPM in Lemma 6 enable the following theorem for the approximate recovery at Stage One.

Theorem 1. (Approximate Recovery at Stage One) Let $\mathbf{x}_i \in \mathbb{R}^N \sim i.i.d \mathcal{BG}(\theta)$ with $\theta \in (\frac{1}{N}, \frac{1}{12}\sqrt{\frac{\pi}{2}})$ and $\mathbf{y}_i = \mathbf{D}^* \mathbf{x}_i^*$, $i = 1, \dots, L$, with $\mathbf{D}^* = \mathbf{I}$. Given an initialization $\mathbf{d}^{(0)} \in \mathcal{S}_{\zeta_0}^{(n\pm)}$, $\forall \zeta_0 \in (0, 1)$ for any $n \in [N]$. Whenever $\epsilon \in (0, \frac{c_3(1+\zeta_0)N^{\frac{1}{2}}}{\zeta_0 \theta^{\frac{1}{2}} (\log(L) \log(NL))^{3/2}})$ and $L \geq C_3 (\frac{1+\zeta_0}{\zeta_0})^2 \frac{N^5}{\theta^3 \epsilon^2} \log(\frac{(1+\zeta_0)N}{\zeta_0 \theta \epsilon})$, with high probability, the sequence generated by the GPM in (14) converges to a point \mathbf{r} that is close to the true atom $\pm \mathbf{e}_n$ in $\mathcal{S}_{\zeta_0}^{(n\pm)}$ in the sense that

$$\|\mathbf{r} - (\pm \mathbf{e}_n)\| \leq \epsilon, \quad (23)$$

where c_3 and C_3 are some positive constants, and $\mathbf{r} = \lim_{t_1 \rightarrow \infty} \mathbf{d}^{(t_1)}$.

Proof. See Appendix H. □

Theorem 1 concludes that once the initialization falls into one good subset, Stage One can recover an approximated solution at that subset and the approximation error can be made arbitrarily small with sufficiently large number of samples.

4.2 Refined Recovery at Stage Two

After obtaining the approximated solution from Stage One, we then show that Stage Two can refine the solution to be exactly any one of the true atoms in the following theorem.

Theorem 2. (Refine the Result at Stage Two) Let $\mathbf{x}_i \in \mathbb{R}^N \sim i.i.d \mathcal{BG}(\theta)$ with $\theta \in (\frac{1}{N}, \frac{1}{12}\sqrt{\frac{\pi}{2}})$, $\mathbf{y}_i = \mathbf{D}^* \mathbf{x}_i^*$, $i = 1, \dots, L$, with $\mathbf{D}^* = \mathbf{I}$. Suppose \mathbf{r} obtained from Stage One satisfies $\|\mathbf{r} - (\pm \mathbf{e}_n)\| \leq \frac{1}{10}$. For any $n \in [N]$, there exist positive constants c_4, c_5 and C_4 . Whenever $L \geq C_4 N \log(N/\theta)/\theta^2$, with high probability, the sequence $\{\mathbf{d}^{(t_2)}\}_{t_2=0}^{\infty}$ generated by the RPG method in (16) with $\mathbf{d}^{(0)} = \mathbf{r}$, $\tau^{(t_2)} = \eta^{(t_2)} \tau^{(0)}$, $\tau^{(0)} = c_4(\theta^{-3} N^{-4})$, and $\eta \in [\sqrt{1 - c_5 \theta^{-2} N^{-4}}, 1]$ converges to the target solution in the sense that

$$\lim_{t_2 \rightarrow \infty} \|\|\mathbf{r}\|_{\infty} \mathbf{d}^{(t_2)} - (\pm \mathbf{e}_n)\| = 0. \quad (24)$$

Proof. The proof can be done in a similar way to the proof of [32, Lemma SM 4.7, Lemma SM 4.9]. □

Remark 2. The $\|\mathbf{r}\|_{\infty}$ in (24) is eliminated by the normalization after the convergence of Stage Two, as explained after (16).

4.3 HRP Exactly Recovers One Atom with Finite Data Samples

The results in Theorem 1 and Theorem 2 hold when the initialization falls in any one of the good subsets, hence choosing an initialization within one of the good subsets is required for the exact recovery of one atom. Fortunately, as shown in [4, 32], uniformly random initialization over the sphere falls into one of the $2N$ good subsets $\{\mathcal{S}_{\zeta_0=\frac{1}{5\log N}}^{(n\pm)}, \forall n \in [N]\}$ with a probability of at least $1/2$. Hence, a few random initializations will guarantee that at least one of these initializations falls in one of the good subsets, with high probability.

Finally, we summarize the statement for exact recovery of one atom in the following theorem.

Theorem 3. (*HRP Exactly Recovers One Atom with Finite Data Samples*) Let $\mathbf{x}_i \in \mathbb{R}^N \sim^{i.i.d} \mathcal{BG}(\theta)$ with $\theta \in (\frac{1}{N}, \frac{1}{12}\sqrt{\frac{\pi}{2}})$ and $\mathbf{y}_i = \mathbf{D}^* \mathbf{x}_i^*, i = 1, \dots, L$, with $\mathbf{D}^* = \mathbf{I}$. There exist some positive constants C_5 and C_6 . Whenever $L \geq C_5 \theta^{-3} N^5 \log(N/\theta)$, with high probability, HRP can recover any one of the atoms in the true dictionary in the sense that

$$\|\hat{\mathbf{d}} - \mathbf{d}^*\| = 0, \quad (25)$$

with $R > C_6 \log N$ times uniformly random initialization over the sphere.

Proof. Proof can be done by summarizing Theorem 1, Theorem 2 and the proof of [4, Theorem 3.10]. \square

5 Experiments

This section provides experiments demonstrating the efficiency of our scheme against state-of-the-art prior works. All the experiments are conducted in MATLAB 2019b with a 3.6 GHz Intel quad-core i7 processor.

5.1 List of Methods

The methods adopted in the experiments are listed as follows.

- **Proposed scheme** (Proposed): Proposed denotes the two-stage scheme in this work, where the parameters for Stage Two are fixed to be $\tau^{(t_2)} = \eta \tau^{(t_2-1)}$, $\tau^{(0)} = 0.1$ and $\eta = 0.8$ in all the experiments.
- **Baseline 1** (K-SVD) [14, 19]: K-SVD denotes the efficient K-SVD implementation provided in the Matlab toolbox KSVD-Box v13 ¹.
- **Baseline 2** (SPAMS) [21, 22]: SPAMS denotes the SPArse Modeling Software (SPAMS)² for efficient dictionary learning. In the simulation, we adopt version 2.6 for Matlab and directly use the codes provided at http://spams-devel.gforge.inria.fr/doc/html/doc_spams004.html#sec5.
- **Baseline 3** (TransLearn) [18]: TransLearn denotes the sparse transform learning method proposed in [18]. In the simulation, we adopt the same parameters as those provided in [18, Section V-A-2)] for the orthogonal dictionary case.
- **Baseline 4** (*logcosh*-RTR) [1, 2]: *logcosh*-RTR denotes the two-stage atom-by-atom method proposed in [1, 2] with the first stage solving a *logcosh* objective by the Riemannian trust region algorithm (RTR). The overall dictionary is recovered via deflation [2, Section III]. In the simulation, we directly use the codes provided at https://github.com/sunju/dl_focm, where the true dictionary is required.
- **Baseline 5** (ℓ_1 -RGD) [4]: ℓ_1 -RGD denotes the method proposed in [4] with the $\|\cdot\|_1$ sparsity-promoting function in Problem (2) and solved by the Riemannian subgradient method atom-by-atom. The overall dictionary is recovered by $5N \log N$ random runs. In the simulation, we directly use the codes provided at https://github.com/sunju/ODL_L1, where the true dictionary is required.
- **Baseline 6** (ℓ_4 -MSP) [5]: ℓ_4 -MSP denotes the method proposed in [5] with the $-\|\cdot\|_4^4$ sparsity-promoting function in Problem (2) and solved by the MSP method.
- **Baseline 7** (ℓ_3 -s1): ℓ_3 -s1 refers to using only the Stage One in the proposed scheme to recover the dictionary.

¹<https://www.cs.technion.ac.il/~ronrubin/software.html>

²<http://spams-devel.gforge.inria.fr>

5.2 Experiments with Synthetic Data

5.2.1 Experiment settings

For all synthetic experiments, we generate the measurements $\mathbf{y}_i = \mathbf{D}^* \mathbf{x}_i^*$, $i = 1, \dots, L$, with the ground truth dictionary \mathbf{D}^* drawn randomly from the orthogonal group $\mathbb{O}(N)$ by applying QR decomposition to random matrix with i.i.d normal elements. The sparse signals $\mathbf{x}_i^* \in \mathbb{R}^N$, $i = 1, \dots, L$, are drawn from the i.i.d. Bernoulli-Gaussian distribution, i.e., $\mathbf{x}_i^* \sim^{i.i.d} \mathcal{BG}(\theta)$, $i = 1, \dots, L$. In the experiments, the sparse-coding target of Baseline 1 (K-SVD) and the desired sparsity level of Baseline 3 (TransLearn) are set to be the true average sparsity θN , which means they are assumed to have the prior knowledge of the true sparsity level.

5.2.2 Empirical sample complexity of the proposed scheme

In Fig. 7, we verify the empirical sample complexity by showing the empirical success rates for recovery by the proposed scheme on both the orthogonal group and the sphere. In the simulation, the sample sizes are set at $L = 10N^{\{0.5, 1, 1.5, 2, 2.5\}}$, and the sparsity levels are at $\theta = 0.2, 0.5$. The recovery metric for the orthogonal group is $\left(\sqrt{\min_{\mathbf{J} \in \mathcal{J}} \frac{\|\hat{\mathbf{D}} - \mathbf{D}^* \mathbf{J}\|_F^2}{\|\mathbf{D}^* \mathbf{J}\|_F^2}} \right) < 10^{-3}$, where $\mathcal{J} = \{\Sigma \Pi | \Pi \in \mathcal{P}, \Sigma \in \mathcal{X}\}$ is the set containing all the N dimensional sign-permutation matrices. Specifically, \mathcal{P} contains all the permutation matrices and \mathcal{X} contains all the diagonal matrices whose diagonal elements are ± 1 . The recovery metric for the sphere is $\left(\sqrt{\min_{\mathbf{e} \in \mathcal{E}} \frac{\|\hat{\mathbf{d}} - \mathbf{D}^* \mathbf{e}\|_F^2}{\|\mathbf{D}^* \mathbf{e}\|_F^2}} \right) < 10^{-3}$, where $\mathcal{E} = \{\pm \mathbf{e}_n, n \in [N]\}$. Each curve is generated from 10 Monte Carlo trials, corresponding to re-sampling the sparse codes 10 times with respect to a fixed random true dictionary. The results in Fig. 7 suggest that the proposed scheme works well with the sample complexity at $\tilde{O}(N^2)$ to recover the whole dictionary when applied over the orthogonal group, and any of the true atoms when applied over the sphere³. The empirical result matches the conjectured sample complexity in [4, 45], which shows that the sample complexity from our theory, $\tilde{O}(N^5)$, is amid the suboptimal sample complexity results, e.g., $\tilde{O}(N^4)$ [4, Theorem 3.8], $\tilde{O}(N^3)$ [2, Theorem 3].

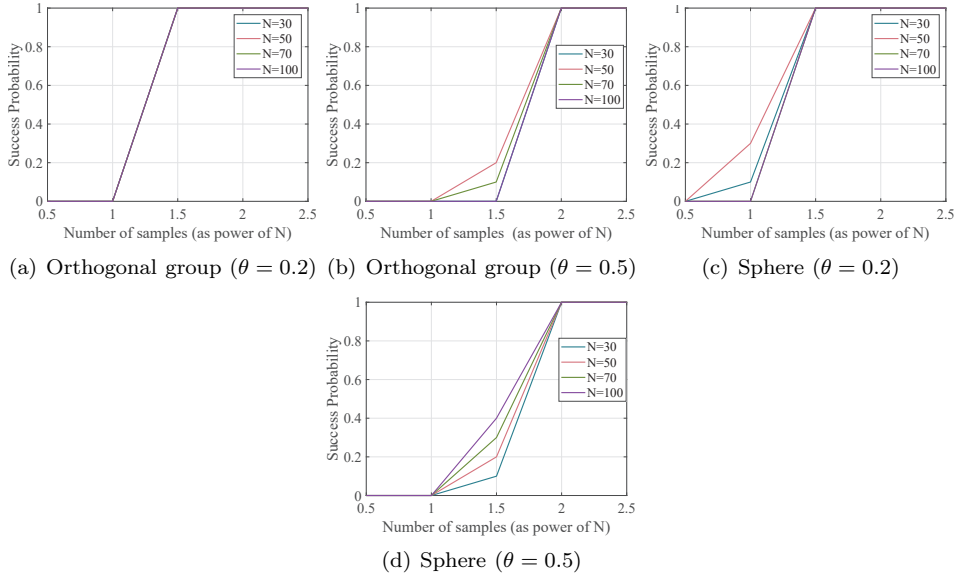


Figure 7: Empirical success rates of recovery of the proposed scheme. Each curve is generated from 10 Monte Carlo trials, corresponding to re-sampling the sparse codes 10 times with respect to a fixed random true dictionary. The top row is for the recovery over the orthogonal group, and the bottom row is for the recovery over the sphere. Left to right columns: $\theta = 0.2, 0.5$, respectively.

³The $\tilde{O}(\cdot)$ notation ignores the dependency on logarithmic terms and other factors.

5.2.3 Dictionary recovery performance comparison

To evaluate the dictionary recovery performance, the accuracy of an estimated dictionary \hat{D} is quantified using the relative RMSE:

$$\text{RMSE} = \sqrt{\min_{J \in \mathcal{J}} \frac{\|\hat{D} - D^* J\|_F^2}{\|D^* J\|_F^2}}, \quad (26)$$

where $\mathcal{J} = \{\Sigma \Pi | \Pi \in \mathcal{P}, \Sigma \in \mathcal{X}\}$ defined in the same way as that in subsection 5.2.2. Fig. 8 shows the RMSE results averaged over 50 Monte Carlo trials under various sparsity levels θ and sample sizes L with a fixed dictionary size $N = 20$. The results demonstrate that the proposed method and Baseline 4 (*logcosh*-RTR) are the two methods with the best dictionary recovery performance. In addition, the proposed method slightly outperforms Baseline 4 under a larger value of the sparsity level ($\theta > 0.4$).

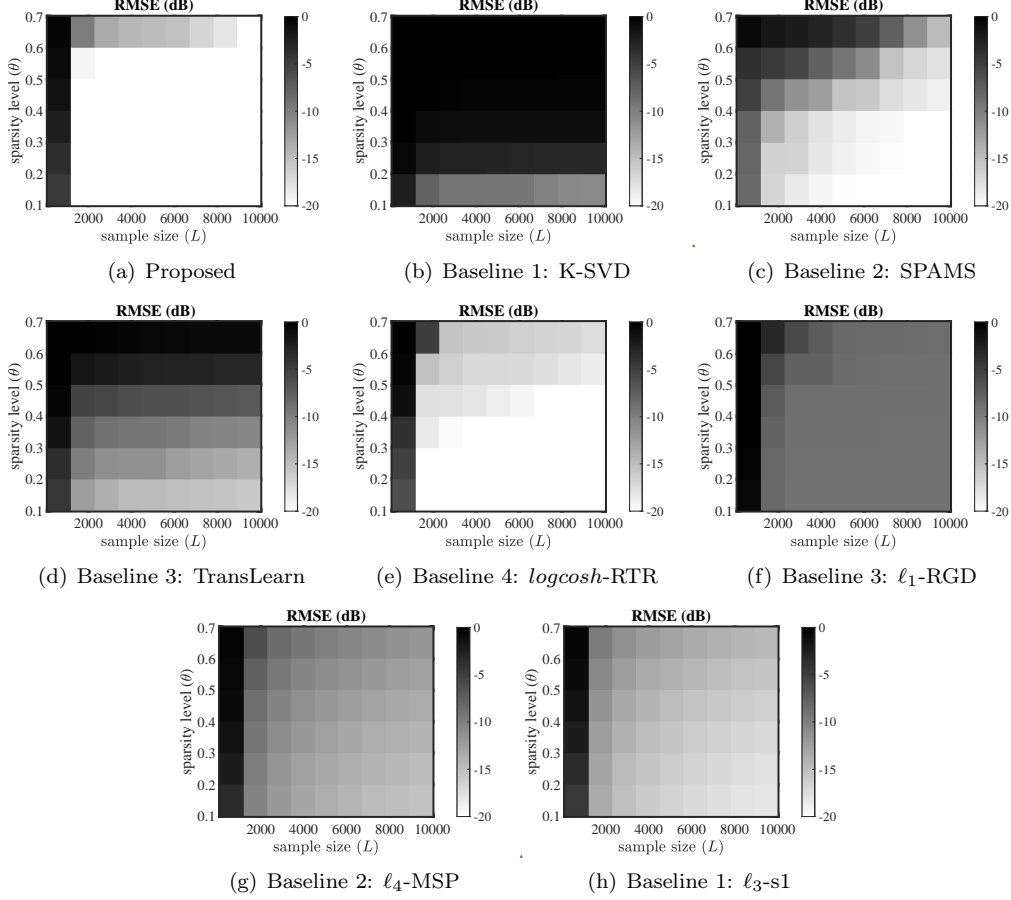


Figure 8: RMSE performance comparison on synthetic data.

5.2.4 Execution time comparison

To evaluate the computational efficiency of the proposed method, we show the CPU time comparison against the dictionary size N and the sample size L in Table 1 and Table 2. Each result is averaged over 50 Monte Carlo trials. We see that solely using Stage One of the proposed method, i.e., Baseline 7 (ℓ_3 -s1), achieves the shortest CPU time, and the proposed scheme has the second to the shortest CPU time with a superior dictionary recovery performance, as indicated in Fig. 8.

5.3 Experiments with Real-world Data

To evaluate the robustness of the proposed method, we conduct experiments on sensor data compression for WSNs. In a typical WSN, there is a data center (DC) to collect sensor readings and transmit the data to the central server for further processing. Due to the limited communication capability of the

Table 1: CPU time comparison with $L = 1000, \theta = 0.2$ and different N

N	10	20	40	50
Proposed	0.010s	0.014s	0.03s	0.04s
K-SVD [19]	0.04s	0.04s	0.10s	0.14s
SPAMS [21, 22]	0.54s	1.45s	4.48s	6.82s
TransLearn [18]	3.64s	5.80s	12.38s	18.92s
<i>logcosh</i> -RTR [2]	22.60s	51.70s	128.13s	127.61s
ℓ_1 -RGD [4]	0.051s	0.26	2.32s	5.15s
ℓ_4 -MSP [5]	0.02s	0.04s	0.09s	0.11s
ℓ_3 -s1	0.006s	0.010	0.02s	0.03s

Table 2: CPU time comparison with $N = 20, \theta = 0.2$ and different L

L	100	2300	4500	10000
Proposed	0.005s	0.019s	0.023s	0.09s
K-SVD [19]	0.02s	0.08s	0.14s	0.30s
SPAMS [21, 22]	0.35s	1.58s	1.74s	2.02s
TransLearn [18]	1.95s	13.87s	23.36s	82.73s
<i>logcosh</i> -RTR [2]	49.25s	50.59s	54.87s	287.20s
ℓ_1 -RGD [4]	0.23s	0.29s	0.34s	2.47s
ℓ_4 -MSP [5]	0.01s	0.09s	0.16s	0.36s
ℓ_3 -s1	0.005s	0.016s	0.019s	0.07s

DC, efficient data compression is required. In a realistic scenario, low-cost sensors may fail to report data, which causes a missing data issue in the system, as shown in Fig. 9.

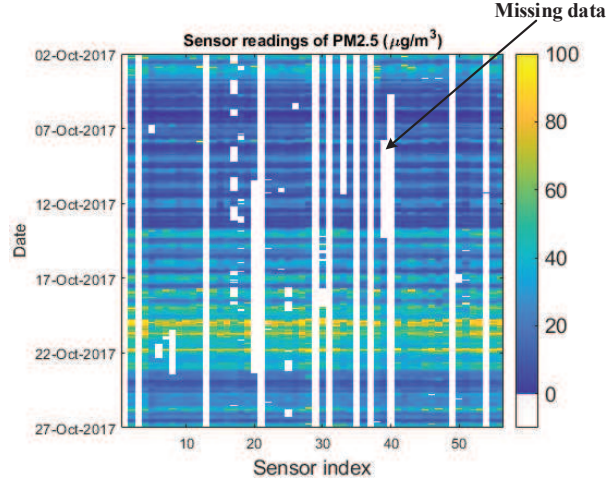


Figure 9: Raw data of the concentration of PM2.5 from 56 sensors in October, 2017 from Krakow, Poland [46]. The missing data in the dataset are set to -10 for visualization.

In the following, we will show that our scheme is not only efficient in compressing the sensor readings but robust to the missing data issue in the sensor datasets [46]. In the experiment, sensor readings $\mathbf{y}_i \in \mathbb{R}^{56}$ are sampled at time index i from 56 sensors located at different places. The missing data at each sample time are first filled with the mean value at that time. Then, the 56×744 readings, $\{\mathbf{y}_i\}_{i=1}^{744}$, are sent to the sparse coding methods. After obtaining the dictionary $\hat{\mathbf{D}} \in \mathbb{O}(56)$ and the sparse code $\hat{\mathbf{x}}_i \in \mathbb{R}^{56}, \forall i = 1, \dots, 744$, we can obtain $\hat{\mathbf{y}}_i$ by $\hat{\mathbf{y}}_i = \hat{\mathbf{D}}\hat{\mathbf{x}}_i$. We compare the RMSE and CPU time under different compression ratios. The RMSE and compression ratio in this real-world sensor data compression task are defined as

$$\text{RMSE} = \sqrt{\frac{\sum_{i=1}^{744} (\hat{\mathbf{y}}_i(\Lambda) - \mathbf{y}_i(\Lambda))^2}{\sum_{i=1}^{744} (\mathbf{y}_i(\Lambda))^2}},$$

$$\text{compression ratio} = \lfloor \frac{56}{T_0} \rfloor,$$

where Λ denotes the complementary set of the indices for the missing data. As shown by the results in Table 3, the proposed method and Stage One of our proposed method enjoy the fastest implementation time ($< 0.1\text{s}$) and the proposed two-stage scheme achieves a superior RMSE performance on this real-world data compression task.

Table 3: The performance of different methods for compressing sensor readings of PM2.5 in October, 2017 from Krakow, Poland [46]

Compression ratio	11 ($T_0 = 5$)		8 ($T_0 = 7$)		5 ($T_0 = 11$)		3 ($T_0 = 18$)		2 ($T_0 = 28$)	
Methods *	Time	RMSE	Time	RMSE	Time	RMSE	Time	RMSE	Time	RMSE
Proposed	0.05s	9.42%	0.05s	8.10%	0.05s	6.22%	0.05s	4.07%	0.05s	2.13%
K-SVD [19]	0.07s	18.55%	0.09s	15.68%	0.12s	8.57%	0.59s	6.99%	0.41s	4.04%
SPAMS [21, 22]	46.97s	26.03%	46.97s	20.35%	46.97s	13.50%	46.97s	8.16%	46.97s	4.36%
TransLearn [18]	17.91s	92.45%	16.35s	75.49%	16.51s	75.00%	16.31s	73.28%	16.41s	65.05%
<i>logcosh</i> -RTR [2]	1704s	10.19%	1704s	8.59%	1704s	6.44%	1704s	4.09%	1704s	2.32%
ℓ_1 -RGD [4]	17.30s	11.42%	17.30s	9.94%	17.30s	7.91%	17.30s	5.56%	17.30s	3.26%
ℓ_4 -MSP [5]	0.19s	10.18%	0.19s	8.83%	0.19s	6.93%	0.19s	4.60%	0.19s	2.44%
ℓ_3 -s1	0.04s	9.58%	0.04s	8.20%	0.04s	6.32%	0.04s	4.18%	0.04s	2.18%

* The sparse-coding target for K-SVD and the desired sparsity level for TransLearn are set to be $56T_0$; The λ for SPAMS is tuned to be 0.002 for a better performance; We adopt the deflation in ℓ_1 -RGD to recovery the whole dictionary for it to achieve a better performance; Since both *logcosh*-RTR and ℓ_1 -RGD require the true dictionary as an input, we set the true dictionary to be the result from the proposed method for both methods.

6 Conclusion

In this paper, we proposed a novel HRP sparse coding scheme that facilitates fast implementation for a superb dictionary recovery performance under a finite number of samples, without atom-by-atom calculation. The theoretical interpretation is also established. Experiments on both synthetic and real-world data verify the efficiency and the effectiveness of the proposed scheme. Future focus on the application aspect includes the distributed and online version of the proposed scheme. Since the theoretical results, e.g., the sample complexity and the convergence rate, in this work are suboptimal compared to the numerical simulation, further work will also focus on pursuing tighter theoretical results.

A Notations and Technical Lemmas

A.1 Notations

A.1.1 Bernoulli-Gaussian random variable

The random vector $\mathbf{x} \in \mathbb{R}^N$ with i.i.d Bernoulli-Gaussian elements can be expressed as

$$\mathbf{x} = \mathbf{b} \odot \mathbf{g}. \quad (27)$$

We have $\mathbf{b} \in \mathbb{R}^N$ with elements $\{b_j\} \sim^{i.i.d} \text{Ber}(\theta) \forall j$ and $\mathbf{g} \in \mathbb{R}^N$ with elements $\{g_j\} \sim^{i.i.d} \mathcal{N}(0, 1) \quad \forall j$. Ω is used to denote the generic support set of \mathbf{b} .

A.1.2 High-order absolute moments of the Gaussian random variable

The p -th-order central absolute moment of Gaussian random variable $g \sim \mathcal{N}(0, \sigma^2)$ is

$$\mathbb{E}[|g|^p] = \sigma^p \frac{2^{p/2} \Gamma(\frac{p+1}{2})}{\sqrt{\pi}}. \quad (28)$$

In the following, we denote $\gamma_p = \frac{2^{p/2} \Gamma(\frac{p+1}{2})}{\sqrt{\pi}}$ for simplicity.

A.1.3 Riemannian gradient over sphere

Given a point $\mathbf{d} \in \mathbb{S}^N$, the Riemannian gradient of $f(\mathbf{d})$ at \mathbf{d} is obtained by

$$\nabla_{grad} f(\mathbf{d}) = (\mathbf{I} - \mathbf{d}\mathbf{d}^T) \nabla f(\mathbf{d}). \quad (29)$$

A.2 Technical Lemmas

Lemma 7. (Expectation of ℓ_p norm for Bernoulli-Gaussian vectors) If the random vector $\mathbf{x} \in \mathbb{R}^N$ is with i.i.d Bernoulli-Gaussian elements, then we have

$$\begin{aligned} \mathbb{E}_{\mathbf{x}}[\|\mathbf{d}^T \mathbf{x}\|_p^p] &= \mathbb{E}_{\mathbf{b}, \mathbf{g}}[\|\mathbf{d}^T (\mathbf{b} \odot \mathbf{g})\|_p^p] \\ &= \mathbb{E}_{\mathbf{b}, \mathbf{g}}[\|(\mathbf{d} \odot \mathbf{b})^T \mathbf{g}\|_p^p] \stackrel{(a)}{=} \gamma_p \mathbb{E}_{\Omega}[\|\mathbf{d}_{\Omega}\|_p^p] \stackrel{(b)}{\leq} \gamma_p \theta, \end{aligned} \quad (30)$$

where (a) is because of the rotation-invariant property of the Gaussian random vectors, and (b) is obtained from [7, Lemma B.1].

B Proof of Lemma 1

- If $\Delta = \mathbf{X} \mathcal{S}_{skew}(N)$, then $\Delta = \mathbf{X}(\mathbf{A} - \mathbf{A}^T)$, since any matrix $\Omega \in \mathcal{S}_{skew}(N)$ can be represented by $\Omega = (\mathbf{A} - \mathbf{A}^T)$ with $\mathbf{A} \in \mathbb{R}^N$. Therefore, $(\mathbf{X} + \Delta)^T \mathbf{X} + (\mathbf{X} + \Delta) \mathbf{X}^T = 2\mathbf{I}$.
- If $\mathbf{Z}^T \mathbf{X} + \mathbf{Z} \mathbf{X}^T = 2\mathbf{I}$, let $\Delta = \mathbf{X} \Omega$, we have $\mathbf{Z}^T \mathbf{X} + \mathbf{Z} \mathbf{X}^T = 2\mathbf{I}$. Then we have $(\mathbf{X} + \Delta)^T \mathbf{X} + (\mathbf{X} + \Delta) \mathbf{X}^T = 2\mathbf{I}$. Finally we have $\Omega + \Omega^T = \mathbf{0}$. Therefore, $\Omega \in \mathcal{S}_{skew}(N)$, and $\Delta = \mathbf{X} \mathcal{S}_{skew}(N)$.

C Proof of Lemma 2

C.1 Concentration of Function Value

Since $\{\mathbf{x}_i\}_{i=1}^L$ are i.i.d with each element $x_{i,j} \sim_{i.i.d} \mathcal{BG}(\theta)$, it is easy to verify that $x_{i,j} \forall i = 1, \dots, L; j = 1, \dots, N$ has a sub-Gaussian tail in the sense that $\Pr[|x_{i,j}| \geq t] \leq e^{-\frac{t^2}{2}}$, and $\|\mathbf{d}^T \mathbf{x}_i\|_3^3$ has a heavy tail in the sense that $\Pr[\|\mathbf{d}^T \mathbf{x}_i\|_3^3 \geq t] \leq 2e^{-C\sqrt{t}}, \forall i = 1, \dots, L$. Therefore, we show the proof by checking the conditions in [30, Corollary F.2]. Define

$$g_{\mathbf{d}}(\mathbf{x}_i) = -\|\mathbf{d}^T \mathbf{x}_i\|_3^3. \quad (31)$$

We have that $\mathbb{E}_{\mathbf{x}_i}[g_{\mathbf{d}}(\mathbf{x}_i)]$ is bounded and Lipschitz by (32) and (33), as shown in the following:

$$\begin{aligned} \|\mathbb{E}_{\mathbf{x}_i}[g_{\mathbf{d}}(\mathbf{x}_i)]\| &= \gamma_3 \mathbb{E}_{\Omega}[\|(\mathbf{d}^T)_{\Omega}\|^3] \stackrel{(b)}{\leq} \gamma_3 \mathbb{E}_{\Omega}[\|(\mathbf{d}^T)_{\Omega}\|^2] = \gamma_3 \theta, \end{aligned} \quad (32)$$

where (a) is due to Lemma 7, (b) is because of $\|(\mathbf{d}^T)_{\Omega}\| \leq 1$, and the equality holds only if $\|\mathbf{d}^T\|_0 = 1$. We also have

$$\begin{aligned} \|\mathbb{E}_{\mathbf{x}_i}[g_{\mathbf{d}_1}(\mathbf{x}_i)] - \mathbb{E}_{\mathbf{x}_i}[g_{\mathbf{d}_2}(\mathbf{x}_i)]\| &= \gamma_3 \|\mathbb{E}_{\Omega}[\|(\mathbf{d}_1^T)_{\Omega}\|^3] - \mathbb{E}_{\Omega}[\|(\mathbf{d}_2^T)_{\Omega}\|^3]\| \\ &\leq \gamma_3 \mathbb{E}_{\Omega}[\|(\mathbf{d}_1^T)_{\Omega}\|^3 - \|(\mathbf{d}_2^T)_{\Omega}\|^3] \leq 4\gamma_3 \|\mathbf{d}_1 - \mathbf{d}_2\|. \end{aligned} \quad (33)$$

Then, consider $\bar{\mathbf{x}}_i$ as a truncation of \mathbf{x}_i , such that

$$\mathbf{x}_i = \bar{\mathbf{x}}_i + \hat{\mathbf{x}}_i, \quad \bar{x}_{i,j} = \begin{cases} x_{i,j}, & \text{if } |x_{i,j}| \leq B \\ 0, & \text{otherwise,} \end{cases} \quad (34)$$

with $B = 2\sqrt{\log(NL)}$. For the truncated vector $\bar{\mathbf{x}}_i$, we have

$$\begin{aligned} \|g_{\mathbf{d}}(\bar{\mathbf{x}}_i)\| &= \|\mathbf{d}^T \bar{\mathbf{x}}_i\|_3^3 \leq \|\mathbf{d}\|^3 \|\bar{\mathbf{x}}_i\|^3 \leq \|\bar{\mathbf{x}}_i\|^3 \\ &\leq (B^2 \|\bar{\mathbf{x}}_i\|_0)^{\frac{3}{2}} = (4B^2 \theta N \log L)^{\frac{3}{2}}, \end{aligned} \quad (35)$$

with a probability of at least $1 - L^{-2\theta N}$. The last inequality follows [47, Lemma A.4]. In addition, we have

$$\begin{aligned} \mathbb{E}_{\bar{\mathbf{x}}_i}[\|g_{\mathbf{d}}(\bar{\mathbf{x}}_i)\|^2] &\leq \mathbb{E}_{\mathbf{x}_i}[\|g_{\mathbf{d}}(\mathbf{x}_i)\|^2] = \gamma_6 \mathbb{E}_{\Omega}[\|(\mathbf{d}^T)_{\Omega}\|^6] \\ &\leq \gamma_6 \theta. \end{aligned} \quad (36)$$

Furthermore, we have

$$\begin{aligned} \|g_{\mathbf{d}_1}(\bar{\mathbf{x}}_i) - g_{\mathbf{d}_2}(\bar{\mathbf{x}}_i)\| &\leq 3\|\mathbf{d}_1 - \mathbf{d}_2\|^3 \|\bar{\mathbf{x}}_i\|^3 \\ &\leq 3(4B^2\theta N \log L)^{\frac{3}{2}} \|\mathbf{d}_1 - \mathbf{d}_2\|. \end{aligned} \quad (37)$$

Summarizing the results from (32),(33),(35),(36), and (37), we obtain

$$\begin{aligned} B_f &= \gamma_3\theta, \quad L_f = 4\gamma_3, \quad R_2 = \gamma_6\theta \\ R_1 &= (4B^2\theta N \log L)^{\frac{3}{2}}, \quad \bar{L}_f = 3(4B^2\theta N \log L)^{\frac{3}{2}}. \end{aligned} \quad (38)$$

We also have $\frac{1}{L} \sum_{i=1}^L g_{\mathbf{d}}(\mathbf{x}_i) = f(\mathbf{d})$ and $\mathbb{E}[g_{\mathbf{d}}(\mathbf{x})] = \mathbb{E}[f(\mathbf{d})]$. Substituting values in (38) to [30, Corollary F.2], for any $\delta \in (0, c_{f1}/(N \log(L) \log(NL)\theta^{\frac{1}{3}})^{3/2})$ and $L \geq C_{f1}\delta^{-2}N\theta \log(\frac{(N\theta \log(NL) \log(L))^{3/2}}{\delta})$, we have

$$\Pr\left[\sup_{\mathbf{d} \in \mathbb{S}^{N-1}} \|f(\mathbf{d}) - \mathbb{E}[f(\mathbf{d})]\| \leq \delta\right] \geq 1 - L^{-1}.$$

This finishes the proof.

C.2 Concentration of Riemannian Gradient

Similarly, we define

$$g_{\mathbf{d}}(\mathbf{x}_i) = \nabla_{grad} g(\mathbf{d}) = -3(\mathbf{I} - \mathbf{d}\mathbf{d}^T)(\mathbf{d}^T \mathbf{x}_i) \mathbf{d}^T \mathbf{x}_i, \quad (39)$$

and follow the same procedures as in Section C.1, and we obtain

$$\begin{aligned} B_f &= C_{bf}\theta, \quad L_f = C_{lf}N\theta, \quad R_2 = 9C_{r2}\theta \\ R_1 &= 3(4B^2\theta N \log L)^{\frac{3}{2}}, \quad \bar{L}_f = 12(4B^2\theta N \log L)^{\frac{3}{2}}, \end{aligned} \quad (40)$$

where C_{bf}, C_{lf}, C_{r2} are some absolute constants. Substituting the values in (40) into [30, Corollary F.2], for any $\delta \in (0, c_{d1}/(N \log(L) \log(NL)\theta^{\frac{1}{3}})^{3/2})$ and $L \geq C_{d1}\delta^{-2}N\theta \log(\frac{(N\theta \log(NL) \log(L))^{3/2}}{\delta})$, we have

$$\Pr\left[\sup_{\mathbf{d} \in \mathbb{S}^{N-1}} \|\nabla_{grad} f(\mathbf{d}) - \nabla_{grad} \mathbb{E}[f(\mathbf{d})]\| \leq \delta\right] \geq 1 - L^{-1}.$$

Summarizing the results in C.1 and C.2, we finish the proof.

D Proof of Lemma 3

We first show that if $\mathbf{d} \in \mathcal{S}'$, then \mathbf{d} is the stationary point:

$$\mathcal{S}' = \left\{ \frac{1}{\sqrt{k}} \mathbf{d} : \mathbf{d} \in \{-1, 0, 1\}^N, \|\mathbf{d}\|_0 = k, k \in [N] \right\}. \quad (41)$$

According to Lemma 7 and the interchange of a derivative and an integral, we have $\mathbb{E}[\nabla f(\mathbf{d})] = -3\gamma_3\theta \mathbb{E}_{\Omega}[\|\mathbf{d}_{\Omega}\| \mathbf{d}_{\Omega}]$. Let $\mathbf{d} \in \mathcal{S}'$ with $\|\mathbf{d}\|_0 = k$ for any $k \in [N]$, and define the support of \mathbf{d} as $\Omega_{\mathbf{d}}$. We have, for all $j \in \Omega_{\mathbf{d}}$,

$$\begin{aligned} \mathbf{e}_j^T \mathbb{E}[\nabla f(\mathbf{d})] &= -3\gamma_3\theta d_j \mathbb{E}_{\Omega} \left[\sqrt{d_j^2 + \|\mathbf{d}_{\Omega \setminus \{j\}}\|^2} \right] \\ &= -3\gamma_3 d_j \sum_{i=1}^k \theta^i (1-\theta)^{k-i} \sqrt{i/k} = \chi(\theta, k) d_j, \end{aligned} \quad (42)$$

and for all $j \notin \Omega_{\mathbf{d}}$,

$$\mathbf{e}_j^T \mathbb{E}[\nabla f(\mathbf{d})] = 0. \quad (43)$$

Therefore, we have $\mathbb{E}[\nabla f(\mathbf{d})] = \chi(\theta, k) \mathbf{d}$. Hence, if $\mathbf{d} \in \mathcal{S}'$, we have

$$\nabla_{grad} \mathbb{E}[f(\mathbf{d})] = (\mathbf{I} - \mathbf{d}\mathbf{d}^T) \mathbb{E}[\nabla f(\mathbf{d})] = \mathbf{0}. \quad (44)$$

Then, if $\mathbf{d} \notin \mathcal{S}'$, suppose \mathbf{d} has a maximum absolute value coordinate, n , and another non-zero coordinate, n' , with a strictly smaller absolute value. Going through all the indices $n \in [N], n' \neq n$ in the proof of Lemma 4, we have $\langle \nabla_{grad} \mathbb{E}[f(\mathbf{d})], \frac{1}{d_{n'}} \mathbf{e}_{n'} - \frac{1}{d_n} \mathbf{e}_n \rangle > 0$. This implies that $\nabla_{grad} \mathbb{E}[f(\mathbf{d})] \neq \mathbf{0}$.

Next, we show that $\mathbf{d} = \pm \mathbf{e}_i, \forall i \in [N]$ are the global optimal points by

$$\begin{aligned} \mathbb{E}[f(\mathbf{d})] &= \mathbb{E}\left[-\frac{1}{L} \sum_{i=1}^L \|\mathbf{d}^T \mathbf{y}_i\|_3^3\right] \\ &= \gamma_3 \mathbb{E}_\Omega[-\|\mathbf{d}_\Omega\|^3] \geq \gamma_3 \mathbb{E}_\Omega[-\|\mathbf{d}_\Omega\|^2] = -\theta \gamma_3. \end{aligned} \tag{45}$$

This finishes the proof.

E Proof of Lemma 4

The proof is similar to [4, B.4]. Specifically, for all $n' \in [N], n' \neq N$ and $d_{n'} \neq 0$, we have

$$\begin{aligned} &\langle \nabla_{grad} \mathbb{E}[f(\mathbf{d})], \frac{1}{d_{n'}} \mathbf{e}_{n'} - \frac{1}{d_N} \mathbf{e}_N \rangle \\ &= \langle -3(\mathbf{I} - \mathbf{d}\mathbf{d}^T) \mathbb{E}[\nabla f(\mathbf{d})], \frac{1}{d_{n'}} \mathbf{e}_{n'} - \frac{1}{d_N} \mathbf{e}_N \rangle \\ &= \langle -3\mathbb{E}[\nabla f(\mathbf{d})], \frac{1}{d_{n'}} \mathbf{e}_{n'} - \frac{1}{d_N} \mathbf{e}_N \rangle \\ &= \langle -3\gamma_3 \mathbb{E}_\Omega[\|\mathbf{d}_\Omega\| \mathbf{d}_\Omega], \frac{1}{d_{n'}} \mathbf{e}_{n'} - \frac{1}{d_N} \mathbf{e}_N \rangle \\ &= 3\gamma_3 \theta \mathbb{E}_\Omega \left[\sqrt{d_N^2 + \|\mathbf{d}_{\Omega \setminus \{N\}}\|^2} \right] - \gamma_3 \theta \mathbb{E}_\Omega \left[\sqrt{d_{n'}^2 + \|\mathbf{d}_{\Omega \setminus \{n'\}}\|^2} \right] \\ &= 3\gamma_3 \theta (1 - \theta) \mathbb{E}_\Omega \int_{d_{n'}^2}^{d_N^2} \frac{1}{2} (t + \|\mathbf{d}_{\Omega \setminus \{N, n'\}}\|^2)^{-\frac{1}{2}} dt \\ &\geq \frac{3\gamma_3}{2} \theta (1 - \theta) \frac{\zeta_0}{1 + \zeta_0} d_N^2 \geq \frac{3\gamma_3}{2N} \theta (1 - \theta) \frac{\zeta_0}{1 + \zeta_0}. \end{aligned} \tag{46}$$

This finished the proof.

F Proof of Lemma 5

To prove Lemma 5, we have

$$\begin{aligned} &\langle \nabla_{grad} f(\mathbf{d}), \frac{1}{d_{n'}} \mathbf{e}_{n'} - \frac{1}{d_N} \mathbf{e}_N \rangle \\ &= \langle \nabla_{grad} \mathbb{E}[f(\mathbf{d})] + \nabla_{grad} f(\mathbf{d}) - \nabla_{grad} \mathbb{E}[f(\mathbf{d})], \frac{1}{d_{n'}} \mathbf{e}_{n'} - \frac{1}{d_N} \mathbf{e}_N \rangle \\ &\geq \langle \nabla_{grad} \mathbb{E}[f(\mathbf{d})], \frac{1}{d_{n'}} \mathbf{e}_{n'} - \frac{1}{d_N} \mathbf{e}_N \rangle \\ &\geq \langle \nabla_{grad} \mathbb{E}[f(\mathbf{d})], \frac{1}{d_{n'}} \mathbf{e}_{n'} - \frac{1}{d_N} \mathbf{e}_N \rangle \\ &\quad - \sup_{\mathbf{d} \in \mathbb{S}^{N-1}} \|\nabla_{grad} f(\mathbf{d}) - \nabla_{grad} \mathbb{E}[f(\mathbf{d})]\| \cdot \left\| \frac{1}{d_{n'}} \mathbf{e}_{n'} - \frac{1}{d_N} \mathbf{e}_N \right\|. \end{aligned} \tag{47}$$

Using Lemma 2, we finish the proof.

G Proof of Lemma 6

We first prove that the GPM iteration remains in that subset. Then, we show that the GPM converges to the stationary point in that good subset.

G.1 Sequence Generated by GPM Remains in the Initialized Good Subset

We then prove that the sequence generated by GPM will remain within the subset $\mathcal{S}_{\zeta_0}^{(n+)}$ if $\mathbf{d}^{(0)} \in \mathcal{S}_{\zeta_0}^{(n+)}$. As indicated in [30], we have that the GPM can be regarded as a Riemannian gradient descent with adaptive stepsize $\tau^{(t_1)} = -\frac{1}{(\mathbf{d}^{(t_1)})^T \nabla f(\mathbf{d}^{(t_1)})}$ since

$$\begin{aligned} & \mathcal{P}_{\mathbb{S}^{N-1}}(\mathbf{d}^{(t_1)} - \tau \nabla_{\text{grad}} f(\mathbf{d}^{(t_1)})) \\ &= \mathcal{P}_{\mathbb{S}^{N-1}}(-\tau \mathbf{d}^{(t_1)} + \underbrace{(1 + \tau (\mathbf{d}^{(t_1)})^T \nabla f(\mathbf{d}^{(t_1)}))}_{=0} \mathbf{d}^{(t_1)}) \\ &= \mathcal{P}_{\mathbb{S}^{N-1}}(-\nabla f(\mathbf{d}^{(t_1)})) = \text{Polar}(\nabla f(\mathbf{d}^{(t_1)})), \end{aligned} \quad (48)$$

with $\tau^{(t_1)} = -\frac{1}{(\mathbf{d}^{(t_1)})^T \nabla f(\mathbf{d}^{(t_1)})}$. Without loss of generality, we assume that $\mathbf{d}^{(0)} \in \mathcal{S}_{\zeta_0}^{(N+)}$. Then defining $\mathbf{g} = \nabla_{\text{grad}} f(\mathbf{d})$, we have the following lemma.

Lemma 8. *Let $\mathbf{x}_i \in \mathbb{R}^N$, $\mathbf{x}_i \sim^{i.i.d} \mathcal{BG}(\theta)$ with $\theta \in (\frac{1}{N}, \frac{1}{12}\sqrt{\frac{\pi}{2}})$, $\mathbf{D}^* = \mathbf{I}$, $\mathbf{y}_i = \mathbf{D}^* \mathbf{x}_i^*$, $\forall i$, and $\mathbf{d} \in \mathcal{S}_{\zeta_0}^{(N+)}$, $\zeta_0 \in (0, 1)$. For any $n' \in [N]$, $n' \neq N$, whenever $\delta \in (0, c'_2/(N \log(L) \log(NL)\theta^{\frac{1}{3}})^{3/2})$ and $L \geq C'_2 \delta^{-2} N \theta \log(\frac{(N \theta \log(NL) \log(L))^{3/2}}{\delta})$, we have*

$$\Pr\left[\frac{\tau^{(t_1)}}{1 - \tau^{(t_1)} g_{n'}^{(t_1)}/d_{n'}^{(t_1)}} \geq 1\right] \geq 1 - L^{-1}. \quad (49)$$

Proof. For $\epsilon' > 0$, we have

$$\begin{aligned} & \frac{\tau^{(t_1)}}{1 - \tau^{(t_1)} g_{n'}^{(t_1)}/d_{n'}^{(t_1)}} = -\frac{1}{(\mathbf{d}^{(t_1)})^T \nabla f(\mathbf{d}^{(t_1)})} \\ & \cdot \frac{d_{n'}^{(t_1)} (\mathbf{d}^{(t_1)})^T \nabla f(\mathbf{d}^{(t_1)})}{\mathbf{e}_{n'}^T \nabla f(\mathbf{d}^{(t_1)})} = -\frac{d_{n'}^{(t_1)}}{\mathbf{e}_{n'}^T \nabla f(\mathbf{d}^{(t_1)})} \\ &= \frac{-d_{n'}^{(t_1)}}{\mathbb{E}[\mathbf{e}_{n'}^T \nabla f(\mathbf{d}^{(t_1)})] + \mathbf{e}_{n'}^T \nabla f(\mathbf{d}^{(t_1)}) - \mathbf{e}_{n'}^T \mathbb{E}[\nabla f(\mathbf{d}^{(t_1)})]} \\ &\stackrel{(a)}{\geq} \frac{-d_{n'}^{(t_1)}}{-3\gamma_3 \theta d_{n'}^{(t_1)} \mathbb{E}_{\Omega} \left[\sqrt{(d_{n'}^{(t_1)})^2 + \|\mathbf{d}_{\Omega \setminus \{n'\}}^{(t_1)}\|^2} \right] - d_{n'}^{(t_1)} \epsilon'} \\ &= \frac{1}{3\gamma_3 \theta \mathbb{E}_{\Omega} \left[\sqrt{(d_{n'}^{(t_1)})^2 + \|\mathbf{d}_{\Omega \setminus \{n'\}}^{(t_1)}\|^2} \right] + \epsilon'}, \end{aligned} \quad (50)$$

where (a) is obtained by using a similar concentration technique as in C.1. Specifically, for any $\delta \in (0, c'_2/(N \log(L) \log(NL)\theta^{\frac{1}{3}})^{3/2})$ and $L \geq C'_2 \delta^{-2} N \theta \log(\frac{(N \theta \log(NL) \log(L))^{3/2}}{\delta})$, we have

$$\Pr\left[\sup_{\mathbf{d} \in \mathbb{S}^{N-1}} \|\nabla f(\mathbf{d}) - \nabla \mathbb{E}[f(\mathbf{d})]\| \leq \delta\right] \geq 1 - L^{-1}, \quad (51)$$

where c'_2 and C'_2 are some absolute constants and we further let $\delta = |d_{n'}^{(t_1)}| \epsilon'$. For some sufficiently large N , under the conditions in Lemma 8, we have $\delta \leq (1 - 3\gamma_3 \theta)$. Then, $\frac{\tau^{(t_1)}}{1 - \tau^{(t_1)} g_{n'}^{(t_1)}/d_{n'}^{(t_1)}} \geq 1$ holds true. \square

Suppose $\mathbf{d}^{(t_1)} \in \mathcal{S}_{\zeta_0}^{(N+)}$. For any $n' \neq N$, we have

$$\begin{aligned} & \left(\frac{d_N^{(t_1+1)}}{d_{n'}^{(t_1+1)}}\right)^2 = \left(\frac{d_N^{(t_1)}}{d_{n'}^{(t_1)}}\right)^2 \left(1 + \frac{\tau^{(t_1)}}{1 - \tau^{(t_1)} g_{n'}^{(t_1)}/d_{n'}^{(t_1)}}\right. \\ & \cdot \left.\left(\langle \nabla_{\text{grad}} f(\mathbf{d}^{(t_1)}), \frac{1}{d_{n'}^{(t_1)}} \mathbf{e}_{n'} - \frac{1}{d_N^{(t_1)}} \mathbf{e}_N \rangle\right)^2\right) \\ &\stackrel{(a)}{\geq} \left(\frac{d_N^{(t_1)}}{d_{n'}^{(t_1)}}\right)^2 \left(1 + \frac{1}{2N} \theta (1 - \theta) \frac{\zeta_0}{1 + \zeta_0} - \delta \left\| \frac{1}{d_{n'}^{(t_1)}} \mathbf{e}_{n'} - \frac{1}{d_N^{(t_1)}} \mathbf{e}_N \right\|^2\right), \end{aligned} \quad (52)$$

where (a) is from Lemma 5 and Lemma 8. Since δ can be made arbitrarily small with sufficiently large L with high probability, the result $\mathbf{d}^{(t_1+1)}$ still remains in $\mathcal{S}_{\zeta_0}^{(N+)}$ if $\mathbf{d}^{(0)} \in \mathcal{S}_{\zeta_0}^{(N+)}$ after the t_1 -th iteration of the GPM.

G.2 Sequence Generated by GPM Converges to a Stationary Point

Then, we prove that the GPM can converge to a stationary point of Problem (13) with high probability. Since a sphere is a spacial Stiefel manifold in the sense that we have $\mathbb{S}^{N-1} = St_1(\mathbb{R}^N)$, where $St_K(\mathbb{R}^N) = \{\mathbf{A} \in \mathbb{R}^{N \times K} : \mathbf{A}^T \mathbf{A} = \mathbf{I}\}$. Using our results for the Stiefel manifold in [48, Lemma 2, Theorem 3], we have the following lemma.

Lemma 9. *Under the conditions in Lemma 2, with $\{\mathbf{d}^{(t)}\}_{t=0}^\infty$ being the sequence generated by the GPM with a random initial point $\mathbf{d}^{(0)} \in \{\mathcal{S}_{\zeta_0}^{(n\pm)}, \forall n \in [N]\}$, we have with a probability of at least $1 - L^{-1}$*

$$\lim_{t_1 \rightarrow \infty} \nabla_{grad} f(\mathbf{d}^{(t_1)}) = 0.$$

Proof. Proof can be done by combining the convergence proof in [48, Theorem 3] and the result in Lemma 2 that with high probability that the objective in Problem (13) is bounded. \square

Combining the results in Appendix G.1 and G.2, we complete the proof.

H Proof of Theorem 1

Without loss of generality, we assume $\mathbf{d}^{(0)} \in \mathcal{S}_{\zeta_0}^{(N+)}$, $\zeta_0 \in (0, 1)$. To prove Theorem 1, we first have

$$\begin{aligned} \frac{1}{\left\| \frac{1}{d_{n'}^{(t_1)}} \mathbf{e}_{n'} - \frac{1}{d_N^{(t_1)}} \mathbf{e}_N \right\|} &= \frac{1}{\sqrt{\left(\frac{1}{d_{n'}^{(t_1)}}\right)^2 + \left(\frac{1}{d_N^{(t_1)}}\right)^2}} \\ &\stackrel{(a)}{=} \frac{1}{\sqrt{\left(\frac{1}{c_{n'} d_N^{(t_1)}}\right)^2 + \left(\frac{1}{d_N^{(t_1)}}\right)^2}} \geq \frac{|c_{n'}| d_N^{(t_1)}}{\sqrt{2}}, \end{aligned} \quad (53)$$

where (a) from the fact that we have $|d_{n'}^{(t_1)}| < |d_N^{(t_1)}|$ in set $\mathcal{S}_{\zeta_0}^{(N+)}$, $\zeta_0 \in (0, 1)$ and we define $d_{n'}^{(t_1)} = c_{n'} d_N^{(t_1)}$ where $|c_{n'}| \leq \sqrt{\frac{1}{1+\zeta_0}}$ by the definition of $\mathcal{S}_{\zeta_0}^{(N+)}$, $\zeta_0 \in (0, 1)$. Then, we further have

$$\begin{aligned} \|\mathbf{d}^{(t_1)} - \mathbf{e}_N\|^2 &\stackrel{(a)}{\leq} \frac{\|\mathbf{d}_{-N}^{(t_1)}\|^2}{(d_N^{(t_1)})^2} \leq \|\mathbf{d}_{-N}^{(t_1)}\|^2 N \\ &\stackrel{(b)}{\leq} \max_{n' \in [N], n' \neq N} \frac{(N-1)N}{\left\| \frac{1}{d_{n'}^{(t_1)}} \mathbf{e}_{n'} - \frac{1}{d_N^{(t_1)}} \mathbf{e}_N \right\|^2}, \end{aligned} \quad (54)$$

where (a) is from [7, C2], and (b) is from (53).

On the good events in Lemma 5 and Lemma 6, we have for all $n' \in [N], n' \neq N$,

$$\frac{1}{\left\| \frac{1}{r_{n'}} \mathbf{e}_{n'} - \frac{1}{r_N} \mathbf{e}_N \right\|} \leq \frac{\delta}{\frac{3\gamma_3}{2N} \theta (1-\theta) \frac{\zeta_0}{\zeta_0+1}}. \quad (55)$$

Substituting (55) in (53), we have

$$\|\mathbf{r} - \mathbf{e}_N\| \leq \frac{2N \sqrt{2N(N-1)(1+\zeta_0)} \delta}{3\gamma_3 \theta (1-\theta) \zeta_0}. \quad (56)$$

Letting $\frac{2N \sqrt{2N(N-1)(1+\zeta_0)} \delta}{3\gamma_3 \theta (1-\theta) \zeta_0} = \epsilon$, summarizing the results from Lemma 5 and Lemma 6 and substituting (56) in that result, we finish the proof.

References

- [1] J. Sun, Q. Qu, and J. Wright, “Complete dictionary recovery over the sphere I: Overview and the geometric picture,” *IEEE Trans. Inf. Theory*, vol. 63, no. 2, pp. 853–884, 2017.

- [2] —, “Complete dictionary recovery over the sphere II: Recovery by riemannian trust-region method,” *IEEE Trans. Inf. Theory*, vol. 63, no. 2, pp. 885–914, 2017.
- [3] D. Gilboa, S. Buchanan, and J. Wright, “Efficient dictionary learning with gradient descent,” in *Proc. Int. Conf. Machine Learn.*, ser. Proceedings of Machine Learning Research, vol. 97. PMLR, 09–15 Jun 2019, pp. 2252–2259.
- [4] Y. Bai, Q. Jiang, and J. Sun, “Subgradient descent learns orthogonal dictionaries,” in *Proc. Int. Conf. Learn. Representations*, 2019.
- [5] Y. Zhai, Z. Yang, Z. Liao, J. Wright, and Y. Ma, “Complete dictionary learning via l4-norm maximization over the orthogonal group,” *J. Machine Learn. Res.*, vol. 21, no. 165, pp. 1–68, 2020.
- [6] Y. Zhai, H. Mehta, Z. Zhou, and Y. Ma, “Understanding l4-based dictionary learning: Interpretation, stability, and robustness,” in *Proc. Int. Conf. Learn. Representations*, 2020.
- [7] Y. Shen, Y. Xue, J. Zhang, K. Letaief, and V. Lau, “Complete dictionary learning via ℓ_p -norm maximization,” in *Proc. Conf. Uncertainty in Artif. Intell. (UAI)*, vol. 124. Virtual: PMLR, 03–06 Aug 2020, pp. 280–289.
- [8] J. Wright, A. Y. Yang, A. Ganesh, S. S. Sastry, and Y. Ma, “Robust face recognition via sparse representation,” *IEEE Trans. Pattern Anal. Mach. Intell.*, vol. 31, no. 2, pp. 210–227, 2008.
- [9] X. Li, J. Fang, H. Duan, Z. Chen, and H. Li, “Fast beam alignment for millimeter wave communications: A sparse encoding and phaseless decoding approach,” *IEEE Trans. Signal Process.*, vol. 67, no. 17, pp. 4402–4417, 2019.
- [10] C. Bao, J.-F. Cai, and H. Ji, “Fast sparsity-based orthogonal dictionary learning for image restoration,” in *Proceedings of the IEEE International Conference on Computer Vision*, 2013, pp. 3384–3391.
- [11] X. Tan, W. Roberts, J. Li, and P. Stoica, “Sparse learning via iterative minimization with application to MIMO radar imaging,” *IEEE Trans. Signal Process.*, vol. 59, no. 3, pp. 1088–1101, 2011.
- [12] J. Allen, “Applications of the short time fourier transform to speech processing and spectral analysis,” in *Proc. IEEE Int. Conf. Acoust. Speech and Signal Process. (ICASSP)*, vol. 7. IEEE, 1982, pp. 1012–1015.
- [13] S. Mallat, *A Wavelet Tour of Signal Processing*. Elsevier, 1999.
- [14] M. Aharon, M. Elad, and A. Bruckstein, “K-SVD: An algorithm for designing overcomplete dictionaries for sparse representation,” *IEEE Trans. Signal Process.*, vol. 54, no. 11, pp. 4311–4322, 2006.
- [15] L. Shi and Y. Chi, “Manifold gradient descent solves multi-channel sparse blind deconvolution provably and efficiently,” *arXiv preprint arXiv:1911.11167*, 2019.
- [16] K. Engan, S. O. Aase, and J. H. Husoy, “Method of optimal directions for frame design,” in *Proc. IEEE Int. Conf. Acoust. Speech and Signal Process. (ICASSP)*, vol. 5. IEEE, 1999, pp. 2443–2446.
- [17] C. Bao, H. Ji, Y. Quan, and Z. Shen, “Dictionary learning for sparse coding: Algorithms and convergence analysis,” *IEEE Trans. Pattern Anal. Mach. Intell.*, vol. 38, no. 7, pp. 1356–1369, 2015.
- [18] S. Ravishanker and Y. Bresler, “Learning sparsifying transforms,” *IEEE Trans. Signal Process.*, vol. 61, no. 5, pp. 1072–1086, 2012.
- [19] R. Rubinstein, M. Zibulevsky, and M. Elad, “Efficient implementation of the K-SVD algorithm using batch orthogonal matching pursuit,” Computer Science Department, Technion, Tech. Rep., 2008.
- [20] R. Rubinstein, T. Peleg, and M. Elad, “Analysis K-SVD: A dictionary-learning algorithm for the analysis sparse model,” *IEEE Trans. Signal Process.*, vol. 61, no. 3, pp. 661–677, 2013.
- [21] J. Mairal, F. Bach, J. Ponce, and G. Sapiro, “Online learning for matrix factorization and sparse coding,” *J. Machine Learn. Res.*, vol. 11, no. Jan, pp. 19–60, 2010.

- [22] R. Jenatton, J. Mairal, G. Obozinski, and F. R. Bach, “Proximal methods for sparse hierarchical dictionary learning,” in *Proc. Int. Conf. Machine Learn.*, 2010.
- [23] J. Mairal, F. Bach, and J. Ponce, “Task-driven dictionary learning,” *IEEE Trans. Pattern Anal. Mach. Intell.*, vol. 34, no. 4, pp. 791–804, 2012.
- [24] H. Lee, A. Battle, R. Raina, and A. Y. Ng, “Efficient sparse coding algorithms,” in *Proc. Adv. Neural Inf. Process. Syst.* Citeseer, 2007, pp. 801–808.
- [25] S. Ravishanker and Y. Bresler, “Learning sparsifying transforms for image processing,” in *Proc. Int. Conf. Image Process.* IEEE, 2012, pp. 681–684.
- [26] E. M. Eksioğlu and O. Bayir, “K-svd meets transform learning: transform k-svd,” *IEEE Signal Process. Lett.*, vol. 21, no. 3, pp. 347–351, 2014.
- [27] D. A. Spielman, H. Wang, and J. Wright, “Exact recovery of sparsely-used dictionaries,” in *Proc. Conf. Learn. Theory*, 2012, pp. 37–1.
- [28] R. Vershynin, *High-dimensional probability: An introduction with applications in data science*. Cambridge University Press, 2018, vol. 47.
- [29] Y. Chi, Y. M. Lu, and Y. Chen, “Nonconvex optimization meets low-rank matrix factorization: An overview,” *IEEE Trans. Signal Process.*, vol. 67, no. 20, pp. 5239–5269, 2019.
- [30] Q. Qu, Y. Zhai, X. Li, Y. Zhang, and Z. Zhu, “Geometric analysis of nonconvex optimization landscapes for overcomplete learning,” in *Proc. Int. Conf. Learn. Representations*, 2020.
- [31] Y. Li and Y. Bresler, “Global geometry of multichannel sparse blind deconvolution on the sphere,” in *Proc. Adv. Neural Inf. Process. Syst.*, 2018, pp. 1132–1143.
- [32] Q. Qu, X. Li, and Z. Zhu, “A nonconvex approach for exact and efficient multichannel sparse blind deconvolution,” in *Proc. Adv. Neural Inf. Process. Syst.*, 2019, pp. 4015–4026.
- [33] Y. Li, Y. Chi, H. Zhang, and Y. Liang, “Non-convex low-rank matrix recovery with arbitrary outliers via median-truncated gradient descent,” *Inf. and Inference: A J. of the IMA*, vol. 9, no. 2, pp. 289–325, 2020.
- [34] Y. Chen, Y. Chi, J. Fan, and C. Ma, “Gradient descent with random initialization: Fast global convergence for nonconvex phase retrieval,” *Math. Program.*, vol. 176, no. 1, pp. 5–37, 2019.
- [35] H. Zhang, Y. Chi, and Y. Liang, “Provable non-convex phase retrieval with outliers: Median truncated Wirtinger flow,” in *Proc. Int. Conf. Machine Learn.*, ser. Proceedings of Machine Learning Research, vol. 48. New York, New York, USA: PMLR, 20–22 Jun 2016, pp. 1022–1031.
- [36] R. Ge, J. D. Lee, and T. Ma, “Matrix completion has no spurious local minimum,” in *Proc. Adv. Neural Inf. Process. Syst.*, vol. 29. Curran Associates, Inc., 2016.
- [37] H. Fu, Y. Chi, and Y. Liang, “Guaranteed recovery of one-hidden-layer neural networks via cross entropy,” *IEEE Trans. Signal Process.*, vol. 68, pp. 3225–3235, 2020.
- [38] Z. Chen, Y. Cao, Q. Gu, and T. Zhang, “A generalized neural tangent kernel analysis for two-layer neural networks,” *Proc. Adv. Neural Inf. Process. Syst.*, vol. 33, 2020.
- [39] Y. Chi and Y. M. Lu, “Kaczmarz method for solving quadratic equations,” *IEEE Signal Process. Lett.*, vol. 23, no. 9, pp. 1183–1187, 2016.
- [40] Y. Li, Y. Chi, H. Zhang, and Y. Liang, “Non-convex low-rank matrix recovery from corrupted random linear measurements,” in *Proc. Int. Conf. Sampling Theory and Appl. (SampTA)*, 2017, pp. 134–137.
- [41] M. Elad and M. Aharon, “Image denoising via sparse and redundant representations over learned dictionaries,” *IEEE Trans. on Imag. Process.*, vol. 15, no. 12, pp. 3736–3745, 2006.
- [42] Y. Li and Y. Bresler, “Global geometry of multichannel sparse blind deconvolution on the sphere,” in *Proc. Adv. Neural Inf. Process. Syst.*, 2018, pp. 1132–1143.

- [43] M. Journée, Y. Nesterov, P. Richtárik, and R. Sepulchre, “Generalized power method for sparse principal component analysis,” *J. Machine Learn. Res.*, vol. 11, no. Feb, pp. 517–553, 2010.
- [44] P.-A. Absil, R. Mahony, and R. Sepulchre, *Optimization algorithms on matrix manifolds*. Princeton University Press, 2009.
- [45] T. Schramm and D. Steurer, “Fast and robust tensor decomposition with applications to dictionary learning,” in *Proc. Conf. Learn. Theory*. PMLR, 2017, pp. 1760–1793.
- [46] Airly, “Air quality data from extensive network of sensors: PM1, PM2.5, PM10, temp, pres and hum data for 2017 year from Krakow, Poland.” [Online]. Available: <https://www.kaggle.com/datascienceairly/air-quality-data-from-extensive-network-of-sensors>
- [47] Y. Zhang, H. Kuo, and J. Wright, “Structured local optima in sparse blind deconvolution,” *IEEE Trans. Inf. Theory*, vol. 66, no. 1, pp. 419–452, 2020.
- [48] Y. Xue, Y. Shen, V. Lau, J. Zhang, and K. B. Letaief, “Blind data detection in massive MIMO via ℓ_3 -norm maximization over the Stiefel manifold,” *IEEE Trans. on Wireless Commun.*, pp. 1–1, 2020.